PART I ENERGY STRAGGLING OF ^{4}He BELOW 2.0 MeV IN Al, Ni, Au AND Pt

PART II STUDIES OF THE Ti-W METALLIZATION SYSTEM ON Si

Thesis by

Joe M. Harris

In Partial Fulfillment of the Requirements

For the Degree of

Doctor of Philosophy

California Institute of Technology

Pasadena, California

1976

(Submitted July 16, 1975)

ACKNOWLEDGMENTS

I take this space to express my appreciation to my advisor, Dr. M.-A Nicolet for all the time and effort he has invested on my behalf. Although we were not always in total harmony, to my knowledge he has always been both open and honest. I also thank J. W. Mayer for his initial encouragement and continuing guidance. Space is too short to acknowledge all those to whom I am forever grateful for their assistance and support in the course of this research effort. However, a small group of people exists to whom I am especially indebted, namely the members of the Tiger Toads Football Team, Chemistry Basketball Team, X-Ray Crystallography Hiking Group, Caltech Scuba Club and all those with whom I went skiing. Without those people, especially F. Fronczek, my stay at Caltech would have been much less pleasurable.

I express gratitude to the Kellogg Radiation Laboratory for use of the 3 MeV accelerator and Dr. C. A. Barnes for his very helpful instruction in the operation of this machine. I also thank the Kellogg Machine Shop for letting me use their machinery to build many of the devices I needed.

Finally, I would like to thank the E.E. Department, Physics Department, Applied Physics Department, O.N.R., Tektronix, NASA (JPL) and all those who administer financial support to graduate students for the pittance supplied me during my stay. Furthermore, I thank the E.E. and Applied Physics Departments for allowing me to stimulate the local economy by employing secretaries after hours to type my thesis. This is truly a step forward for student-faculty relations.

Special thanks to Ruth Stratton, Lori Oliver, Carol Norris, Dian Rapchak for typing and helping me prepare this manuscript, and to Anita and John Criticos for helping me proof it. I further thank Rob Gorris for his help in designing and building various devices I used in this work.

Part I

I acknowledge a certain unnamed razor blade company for preparing and characterizing the Pt samples. They also provided some analysis as well as many Cr and Al samples, the data from which were not published; however much was learned from measurements made on these samples. I thank C. H. Wilts and F. B. Humphrey for use of their vacuum evaporator and multiple beam interferometer, and the Hewlett Packard Co. for use of their Tally Step. Also, I thank Dr. Wasserberg for making available his microbalance, although I doubt he was aware of this.

Part II

I acknowledge Ron Nowickie and the Fairchild Semiconductor Corp. for preparation of the Ti-W samples and some analysis. I thank Dr. Drew Evans of the University of Illinois, Urbana for his SEM, EMP, and Auger analysis of the Au/TiW/Si samples and JPL for the use of their SEM and EDAX equipment. Finally, I very much appreciate Dr. S. S. Lau's assistance with this project as well as Dr. S. O. Sampson for use of his Gunier Camera and help with the X-ray analysis. R. Shima and J. Maserjian are to be credited with initially suggesting this study and were a constant source of encouragement during its course.

Abstract

Part I

In recent years, backscattering spectrometry has become an important tool for the analysis of thin films. An inherent limitation, though, is the loss of depth resolution due to energy straggling of the beam. To investigate this, energy straggling of ^4He has been measured in thin films of Ni, Al, Au and Pt. Straggling is roughly proportional to square root of thickness, appears to have a slight energy dependence and generally decreases with decreasing atomic number of the adsorber. The results are compared with predictions of theory and with previous measurements. While Ni measurements are in fair agreement with Bohr's theory, Al measurements are 30% above and Au measurements are 40% below predicted values. The Au and Pt measurements give straggling values which are close to one another.

Part II

MeV backscattering spectrometry and X-ray diffraction are used to investigate the behavior of sputter-deposited Ti-W mixed films on Si substrates. During vacuum anneals at temperatures near 700^oC for several hours, the metallization layer reacts with the substrate. Backscattering analysis shows that the resulting compound layer is uniform in composition and contains Ti, W and Si. The Ti:W ratio in the compound corresponds to that of the deposited metal film. X-ray analyses with Reed and Guinier cameras reveal the presence of the ternary $Ti_xW_{(1-x)}Si_2$ compound. Its composition is unaffected by oxygen contamination during annealing, but the reaction rate is affected. The rate measured on samples with about 15% oxygen contamination after annealing is linear, of

the order of 0.5 Å per second at 725°C, and depends on the crystallographic orientation of the substrate and the dc bias during sputter-deposition of the Ti-W film.

Au layers of about 1000 Å thickness were deposited onto unreacted Ti-W films on Si. When annealed at 400°C these samples underwent a color change, and SEM micrographs of the samples showed that an intricate pattern of fissures which were typically 3μm wide had evolved. Analysis by electron microprobe revealed that Au had segregated preferentially into the fissures. This result suggests that Ti-W is not a barrier to Au-Si intermixing at 400°C.

TABLE OF CONTENTS

PART I

ENERGY STRAGGLING OF ^{4}He BELOW 2.0 MeV IN Al, Ni, Au AND Pt

Part I

INTRODUCTION

Discussion of Backscattering in General

MeV α-particles have been used to probe material since about 1909 when Geiger and Marsden, working under Lord Rutherford, performed a series of classic experiments designed to determine the nature of the atom [1]. Nuclear physicists in the early 50's used He-particle scattering to identify contaminants in their targets, and in 1957 Rubin, Passell and Bailey [2] used nuclear methods as an analytical tool to investigate surfaces; however, during the following ten years, few applications were found for this method. The most widely publicized use of α-particle scattering in an experiment of "non-nuclear" interest was performed on September 9, 1967 when NASA used α-particle backscattering aboard the Surveyor 5 to obtain the first factual information on the chemical composition of the lunar soil [3]. Since then backscattering analysis has been applied to a variety of problems originating in both the scientific and industrial communities. Microanalysis by backscattering spectrometry has, within the past five years, become a familiar part of the literature dealing with thin films and semiconductors.

The popularity and acceptance of this microanalytical tool is evidenced by the number of review articles written in the last few years on the applications of Rutherford backscattering microscopy [4]. Particles with energies ranging from a few keV to MeV have been used for backscattering spectrometry [5]. However, the discussion which follows, unless otherwise noted, deals specifically with ^{4}He projectiles of incident energy between 1 and 2 MeV. Furthermore, backscattering used in

this text implies simple Coulombic scattering through an angle near 180°.

Backscattering analysis is not complicated and the necessary equipment is common to most nuclear laboratories. For many years the monoenergetic beam of He ions was produced by natural radioactive decay, however today most backscattering analysis is performed with the use of an accelerator. This has the primary advantage that the beam energy and beam current can be easily varied to suit the experiment. The beam, which is about 1 mm^2, strikes a target mounted on a holder. The target must be uniform over the beam spot for the analysis to be valid. The target holder used for the measurements reported here was designed to hold up to 12 targets and is rotatable about its vertical axis so that targets can be tilted with respect to the beam (see Fig. 1).

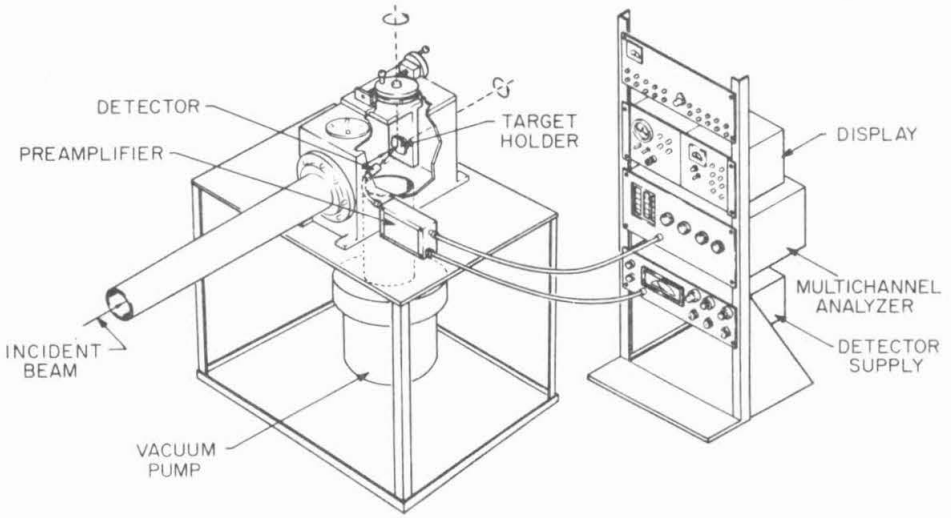

Fig. 1. Schematic showing experimental backscattering setup. 3 MeV Van de Graaff generates the incident beam.

A small fraction, typically one part in 10^9, of the incident beam is backscattered by the target into a detector. The energy-sensitive detector is placed so as to intercept the particles which have been backscattered through the appropriate angle for the experiment being performed. Measurements described in this text were made at a scattering angle of 168° with respect to the incident beam, unless otherwise noted, and with a specially selected high resolution silicon detector. The amplitude of the electrical signals produced by the silicon detector is proportional to the energy of the particle intercepted. These signals are amplified by a low noise preamplifier, a linear amplifier, and finally, a biased amplifier. The linear amplifier has selectable bandwidth which is chosen to give optimum signal to noise ratio, and the biased amplifier shapes the pulses from the linear amplifier so that they can be accepted by a multichannel analyzer. The biased amplifier can also be adjusted to subtract a constant value from incoming pulses and amplify the remainder; this feature is convenient when only those particles in a certain energy range are of interest. A multichannel analyzer accepts the processed pulses from the biased amplifier. It converts each pulse's height into an equivalent address within the memory, known as a channel, and adds one to the total stored in that channel. The analyzer can display its memory which contains a record of the number of pulses in each channel. The display is called a "backscattering spectrum", and once the channels have been calibrated in energy rather than pulse height, the backscattering spectrum becomes an energy spectrum of the particles backscattered into the detector from the target.

Figure 2 shows a backscattering spectrum taken from a target of 2000Å of Pt on SiO_2 . The signal from the SiO_2 has been suppressed by use of the biased amplifier.

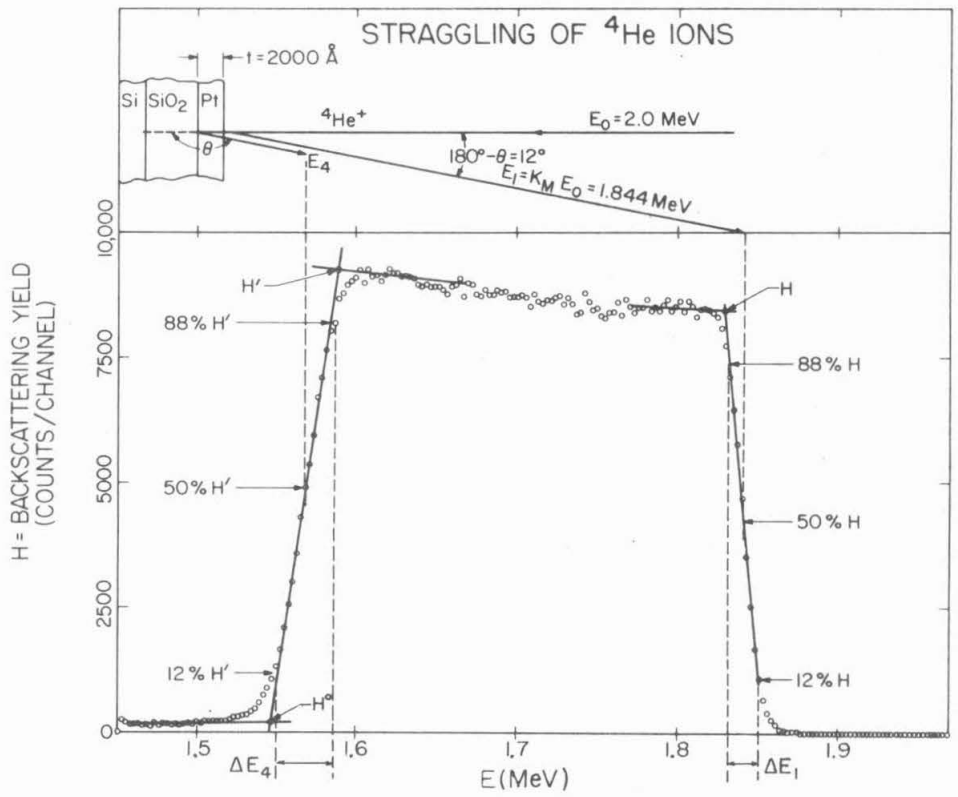

Fig. 2. Typical 2.0 MeV backscattering spectrum of Pt on SiO_2. Substrate signal not shown.

Interpretation of a backscattering spectrum is based on three basic principles. (i) First, the energy of a particle which has undergone Rutherford scattering is proportional to its incident energy. If E_0 is the projectile's incident energy and E' is the projectile's energy after scattering, then

$$E' = E_o K_m \tag{1}$$

where

$$K_m = \frac{m_1 \cos\theta}{m_1 + m_2} + \sqrt{\left(\frac{m_1 \cos\theta}{m_1 + m_2}\right)^2 + \frac{m_2 - m_1}{m_1 + m_2}} \tag{2}$$

θ = the laboratory scattering angle

m_1 = mass of projectile

m_2 = mass of target atom.

and where the subscript 2 in K_{m_2} is normally omitted, since m_2 is usually the variable in Eq. 2.

The formula for K_m is easily derived by applying conservation of energy and momentum to elastic scattering through an angle θ by two bodies of mass m_1 and m_2 respectively [6]. K_m for ^{4}He particles scattered through an angle of 168° from Pt is .922 and from C is .254. The mass of atoms on the surface of a target can be determined by calculating K_m from the measured energy of a projectile backscattered from the surface and using Eq. 2 to determine m_2. The mass resolution is, of course, limited. For instance, a detector has finite energy resolution and one may not be able to determine the energy accurately enough to distinguish between neighboring elements. To improve the energy resolution, it is desirable to get the largest energy loss possible, hence measurements for elemental analysis are made as near 180° as possible with ^{4}He being preferable to lighter projectiles. Furthermore, measurements are typically made at as high an incident energy as possible. Projectiles heavier than ^{4}He are usually impractical, due to reduced detector resolution,

and energies much higher than 2.5 MeV for ^{4}He are frequently outside the Rutherford scattering regime for light targets. It is typically impossible to resolve mass differences less than about 10 a.m.u. for atoms heavier than Sb.

(ii) The second principle basic to backscattering analysis involves target penetration. The projectile penetrates the target and in doing so it loses energy because it collides with the electrons in the target. Nuclear stopping is usually negligible except at very low energies, for instance at 60 keV nuclear stopping of ^{4}He in Cu is less than 3% of the total stopping and decreases at higher energy [38]. The stopping power of a target is given in terms of an energy loss per unit length, dE/dx, and is a function of the incident energy, projectile mass and charge, and target material. Accurate calculations of the stopping power have been successful only for the high energy regime where the projectile's velocity is much greater than the orbital velocities of the atomic electrons of either the incident particle or the target atoms. This regime corresponds to energies greater than about 4 MeV for ^{4}He (1 MeV for ^{1}H) and agreement between experiments and the theory of Bethe-Bloch [7] including corrections [8] is the order of 1% [9]. The stopping power given by the Bethe-Bloch formula is

$$\frac{dE}{dx} = \frac{4\pi e^4 z_1^2}{m_o v^2} N z_2 \left(\ell n \frac{2m_o v^2}{I} - \ell n(1 - \beta^2) - \beta^2 - \frac{C_K}{z_2} \right) \qquad (3)$$

where

N = atomic density

e = 4.803×10^{-10} esu

z_2 = atomic no. of target

z_1 = atomic no. of projectile

m_o = rest mass of electron = $.5488 \times 10^{-3}$ amu

$v = \beta c$ = velocity of projectile

c = velocity of light = 2.997×10^{10} cm/sec

I = geometric-mean of excitation and ionization potential

c_K = correction due to inner shell electrons not participating in the stopping processes

The mean excitation energy is an atomic parameter arrived at by taking the logarithmic average over the excitation energies weighted by the oscillator strengths. With few exceptions, the oscillator strengths are not known well enough to calculate I, so I is usually determined by measurements of dE/dx at energies where c_K/z_2 is small [9]. The correction for non-participating electrons, c_K, have been derived [10, 11, 12] for a number of cases. At extremely relativistic energies ($V \simeq .87c$) polarization of the stopping medium becomes a parameter affecting the stopping processes and the correction term of Sternheimer [13], $-\delta$, is usually included in Eq. 3. However, at extremely high energies the projectile cannot be treated as a point charge and the essentially non-relativistic derivation of Bethe is no longer applicable. A recent treatment of the stopping power at relativistic velocities has been given by Brynjolfsson [14].

At ^{4}He energies lower than about 300 keV the theory of Lindhard and Scharff [15] has been reasonably successful in explaining the linear dependence of stopping power on projectile velocity. The agreement between experiment and calculation, though, is seldom better than 20% or 30%. Like the Bethe-Bloch theory, the L&S theory is based on the Thomas-Fermi model of the atom; however, it contains no adjustable parameters as the Bethe-Bloch theory does.

The intermediate energy regime is the most difficult to treat theoretically because neither the impulse (high energy) nor adiabatic (low energy) approximation is valid. The work of Chu [16] gives probably the best description of the stopping power in this regime. He uses the Hartree-Fock-Slater atomic-wave functions for isolated atoms in the formalism developed by Lindhard and Winther [17]. This calculation explains the experimentally observed stopping power dependence on the atomic number of the target. Furthermore, the Chu calculation yields the square-root of energy dependence at low energy similar to the Lindhardand Scharff theory and gives the $\ell n(E)/E$ dependence of the Bethe-Bloch theory at high energy. The agreement with experiment for ^4He at energies above 1.2 MeV is within 10% for most materials; below 1 MeV experimental results in solids are about 30% lower than theory.

In general the stopping power cannot be determined theoretically to better than about 20% without relying on experimental data to evaluate adjustable parameters. Brice [18] has recently modified and extended Firsov's theory [19] to the higher energy ranges by including three adjustable parameters. This formula of Brice's allows one to fit experimental data with a root-mean square deviation between 1 and 2% over an energy range from 0 to 40 MeV for ^4He. From a practical standpoint, the Brice formula is very useful because it allows one to extrapolate dE/dx to both energies and elements where no measurements exist. Furthermore, the formula gives a simple analytic expression which can easily be used for computer computations. However, when experimental data exist for the desired target and energy range, one is usually better off to use the measured values rather than relying on extrapolation.

The He stopping power has been measured in many elements for the energy range from .5 to 2.0 MeV to an accuracy better than 10%. A recent compilation of measured ^{4}He stopping power is given by Ziegler and Chu [16] and stopping power extrapolated to cover .4 to 4 MeV is given in reference [16] and the Catania Working Data [20]. Stopping data of ^{1}H have been compiled in a number of places [21].

Measuring the energy difference between particles scattered at the surface and those scattered from within the target, one can obtain the depth in the target at which the latter event occurred from the expression

$$x = \frac{(K_m E_o - E_4)}{[S(E_o)]} \qquad \text{(see Fig. 2)} \tag{4}$$

$$[S(E_o)] = K_m \left.\frac{dE}{dx}\right|_{E_{in}} + \frac{1}{\cos\theta} \left.\frac{dE}{dx}\right|_{E_{out}} \tag{5}$$

where

E_o = incident projectile energy

E_4 = exit projectile energy

$[S(E_o)]$ = backscattering energy loss factor for particles with incident energy E_o

x = depth within target from which scattering occurred

K_m = kinematic scattering factor (Eq. 2)

$\left.\frac{dE}{dx}\right|_E$ = stopping power evaluated at energy E

E_{in} = average energy over the incoming path

E_{out} = average energy over the outgoing path

If dE/dx is assumed to be linear function of energy over the energy range of the projectile in the incoming path, namely the range between E_o and E where E is the projectile's energy just before scattering, and dE/dx is also assumed to be linear over the projectile's outgoing path, then E_{in} and E_{out} can be approximated by

$$E_{in} = (E_o + E)/2$$
$$E_{out} = (E_4 + K_m E)/2 \qquad (6)$$

Unfortunately, the value of E depends on the depth of the scattering event and hence must be determined by iteration. For thin targets where $E_o \cong E$ and $E_4 \cong K_m E_o$, Eq. 6 simplifies to

$$E_{in} = E_o$$
$$E_{out} = K_m E_o \qquad (7)$$

The accuracy of this thin-film approximation depends on the incident energy, energy dependence of dE/dx, and of course the depth of the scattering event. For about 1000Å of a medium weight elemental film, such as Ni, the thin film approximation is accurate to within a few percent. However, for heavy thick films ($\sim$ 5000A Pt) at incident energies below about 1.0 MeV, even the linear approximation of Eq. 6 fails and a more rigorous treatment which accounts for the energy dependence of dE/dx is necessary. The uncertainty in the depth is usually limited, in any case, by the energy resolution of the detector or the energy straggling of the beam; for instance, depth resolution for 2.0 MeV He is seldom better than about 200Å for even thin targets,

because solid state detectors seldom have better than 10 keV energy resolution.

Since there are two energy loss mechanisms contributing to the energy distribution of backscattered particles, an ambiguity can arise. For instance, a light element on the surface can produce backscattered particles at the same energy as a heavy element buried within the target. To resolve this ambiguity one need only tilt the target and observe the response of the backscattering spectrum. Tilting the target does not affect the backscattering signal from the surface, however, signals generated by scattering from beneath the surface are shifted to lower energies, since the incoming and outgoing path lengths are increased. It is for this reason that the target holder is designed so that targets can be tilted.

(iii) The final principle necessary to interpret backscattering spectra involves the quantity of backscattering events one observes. The number of backscattering events occurring is proportional to the incident flux of projectiles, atomic density within the target, the target depth probed by the beam, and the cross section for scattering given by

$$H(E_4) = Q\sigma(E)\Omega N\ \delta x \qquad \text{(see Fig. 2)} \qquad (8)$$

$H(E_4)$ = counts in channel at energy E_4 (counts/channel)

Q = total number of incident particles

N = atomic density

δx = thickness of target from which particles backscattered will have energies between $E_4 - E_4/2$ and $E_4 + E_4/2$

δE_4 = energy width of the channel whose counts are being calculated

Ω = solid angle subtended by the detector

$$\sigma(E) = \frac{1}{\Omega} \int_{\substack{\text{over} \\ \Omega}} \frac{d\sigma}{d\Omega}(E) \; d\Omega \tag{9}$$

E = energy of projectile just before scattering

$\frac{d\sigma}{d\Omega}(E)$ = Rutherford differential cross section

Evaluation of Eq. (8) can become rather involved for channels where E_4 corresponds to scattering events lying deep within the target. This is because the $H(E_4)$ depends in two ways on the depth, x, at which the scattering event occurred. First, the energy E of the particle just before the scattering event is given (in the linear approximation) by

$$E = E_o - \left.\frac{dE}{dx}\right|_{E_{in}} x \tag{10}$$

Second, since a channel has an energy width δE_4, scattering events occurring over a finite thickness δx in the target are all counted in that channel and the thickness δx is related to δE_4 by the backscattering energy loss factor evaluated for particles with incident energy E rather than E_o, $[S(E)]$ (Eq. 5). So it is convenient to cast Eq. 8 in terms of E only [21], instead of both E and δx. This gives

$$H(E_4) = Q\sigma(E)\,\Omega N \frac{\delta E_4}{[S(E)]} \frac{(dE/dx)\big|_{K_m}}{(dE/dx)\big|_{E_4}} \tag{11}$$

where $[(S(E)]$ is given by Eq. 5 evaluated at E and the approximations $E_{in} = E$ and $E_{out} = K_m E$ are made because δx is very narrow so the thin

film approximation is justified.

The Rutherford differential cross section can be calculated from first principles and is given in laboratory coordinates by [23]

$$\frac{d\sigma}{d\Omega} = \left(\frac{z_1 z_2 e^2}{2E \sin^2\theta}\right)^2 \frac{\left[\cos\theta + \left[1 - \frac{m_1}{m_2}\sin\theta)^2\right]^{1/2}\right]^2}{\left[1 - \left(\frac{m_1}{m_2}\sin\theta\right)^2\right]^{1/2}} \qquad (12)$$

where

$e = 4.803 \times 10^{-10}$ esu

z_1, m_1 = atomic number and mass of projectile

z_2, m_2 = atomic number and mass of target atom

E = energy of projectile just before scattering

θ = scattering angle of projectile

for $m_2 > m_1$. The Rutherford formula is based on two assumptions. First, that scattering is due to the coulombic interaction of bare nuclei, hence screening due to atomic electrons is not included. Since atomic screening does become a problem for low energy projectiles scattered from heavy atoms, the scattering of the ^{4}He from Au departs from Rutherford by about 12% at 100 keV, however at energies greater than 400 keV the correction is less than 2% [24]. The second assumption is that the projectile is scattered only by coulombic interaction and not by other nuclear forces. This condition breaks down for high energy projectiles on light targets. For instance, a resonance for ^{4}He scattering from ^{16}O at an angle of 164° occurs at 2.4 MeV and the cross section differs from Rutherford scattering by a factor of 2 [25].

The Rutherford cross section for backscattering near 180° is rather small; only about 5 atoms in 10^9 are backscattered into a typical detector at 168° from a 2.0 MeV He beam by 1300Å of Pd. Furthermore, since the cross section is proportional to the atomic number of the scattering atom squared, about 100 times more projectiles are scattered from a heavy atom like Pt than from a light atom like oxygen, other parameters held equal. This introduces a basic limitation. For instance, if an oxygen signal occurs at the same energy as a Pt signal, then the oxygen signal is likely to be totally obscured. Caution must be exercised in the choice of substrate and film thickness for experiments in which light elements are to be detected.

Figure 2 contains a 2.0 MeV ^{4}He backscattering spectrum from a 2000Å thick film of Pt on a SiO_2 substrate. Each of the points corresponds to a channel in the multichannel analyzer. The height of each point corresponds to the number of backscattering events detected within an energy width of 2.6 keV centered at the energy marked on the abscissa.

Introduction to Energy Straggling

The previous section discusses briefly the characteristics of the stopping power, dE/dx. One important facet was omitted, namely that the stopping power is a statistical quantity. As mentioned earlier, projectiles penetrating a target lose energy by collisions with electrons; however, every projectile does not encounter the same

number or type of collision. Imagine that a perfectly monoenergetic beam penetrates a very thin foil and that the particles in the exit beam are detected with a perfect detector. Particles in the exit beam will have an energy distribution, because some particles will either encounter more atoms, or will lose more energy in their collisions, than others. This distribution for He projectiles in the energy range between 1 and 2 MeV is closely approximated by a Gaussian function of energy if the target is not too thick. The stopping power is the most probable energy loss per unit length and can be evaluated by measuring the energy difference between the incident beam and the maximum in the energy profile of the exit beam. The energy straggling is the energy width in the profile of the exit beam. However, no universal agreement exists as to which measure of the profile width is best. Most theorists and a large segment of the physics community give the standard deviation of the energy profile to characterize straggling. Those who use ion beams for microanalysis usually quote straggling in terms of the full width at half maximum (FWHM) of the exit profile. Still others quote straggling as twice the halfwidth at half maximum measured on the high energy side of the profile. If the profile is Gaussian, these various methods of describing straggling are all related to one another by constant factors. If the energy profile is non-Gaussian, and particularly if it is asymmetrical, the various methods are not easily related. Since the measurements reported here were performed in a regime where the energy profiles are very nearly Gaussian, conversion from one method to another is simple (see Appendix II, p. 70.) In this text the value of the FWHM is denoted by ΔE, and that of the standard

deviation by Ω .

Motivation

The discussion of backscattering in the first section implied that the primary limitation to mass and depth resolution was the energy resolution of the detector. This is often true for solid state detectors. However, detection systems using electrostatic and magnetic analyzers are available which have energy resolution from three to four times better than that of a solid state detector. It would seem that one could get a substantial increase in mass and depth resolution by simply using one of these high resolution detection systems.

The mass resolution for surface elements would be enhanced by one of these systems. The depth and mass resolution below the surface depends on the energy straggling incurred by the projectile as well as the detector resolution. The uncertainty in the energy loss due to straggling implies an uncertainty in both the depth to which the projectile penetrated and the mass from which the projectile scattered. Consequently, energy straggling limits the depth and mass resolution irrespective of the detection system.

Experimental straggling data in solids are available for ^{1}H [26], but those for He are scarce [32-34]. Furthermore, the ^{4}He measurements are typically in an energy range above the 1-2 MeV commonly used for backscattering. We have therefore undertaken to measure the energy straggling of ^{4}He below 2.0 MeV for a few elements. The materials were selected as representative of light, medium, and heavy elements.

Complications Arising with Backscattering

The idealized straggling experiment mentioned earlier assumed a perfect detector and a perfectly monoenergetic beam. In practice, neither can be realized. The incident beam profile and the energy response of the detector both contribute to the measured profile of the exit beam. To obtain the contribution made by straggling one must remove both these effects from the energy width of the exit profile. Removal is rather simple though, because the incident beam profile is very nearly a Gaussian function of energy, as are the detector response and the energy profile due to straggling. So the square of the energy width of the exit beam is the sum of the squares of the widths of the contributing parts. Hence, to obtain the straggling squared, one simply subtracts the square of the energy width of the detector response and the square of the energy width of the incident beam profile from the square of the energy width of the measured exit beam profile. This discussion implies that one must know individually the widths of the detector response and the incident profile to perform straggling measurements. However, in practice, these quantities are measured in combination. Generally, one measures the profile of the incident beam with the detector, so the measured energy width of the incident beam is the quadratic sum of the energy width of the incident profile and that of the detector response. Hence, the energy width as measured by the detector can be subtracted in quadrature from the measured energy width in the profile of the exit beam to yield the straggling (see Appendix I, p. 64).

Measurement of the incident profile by backscattering is easy, since particles scattered from the surface of a target like Pt

have an energy profile similar to that of the incident beam and one can obtain the energy width of the scattered beam from the high energy edge of a normal backscattering spectrum. An ordinary backscattering spectrum displays the integral of the profile, rather than the profile itself. Since the profile is nearly Gaussian, this edge is almost an error function and the profile's FWHM is the energy difference between the 12% and 88% height points of the edge. Similarly, the FWHM of the measured exit beam profile is the energy difference between the 12% and 88% height points of the low energy edge. This discussion is valid for any element if certain scattering corrections are made; however, its use here is limited to heavy elements for reasons which will be discussed next. For a more in depth discussion of the above, see Appendix I, p. 64.

Straggling measurements made in backscattering differ in a number of ways from those made in transmission. The most obvious difference is that in backscattering the projectile must traverse the target twice. Hence, path length corrections must be made when comparing transmission and backscattering experiments. A more important distinction exists when straggling measurements are made in backscattering on light elements. A significant portion of the projectile's energy is lost during the elastic collision with a light element, so the incoming and outgoing paths lie in different energy ranges. This makes it difficult to unravel the energy dependence of straggling because the contributions to the measured straggling come from two different energy regimes.

The elastic collisions also modify the beam profile. When a beam scatters from any element, the profile width of the scattered beam is smaller than the profile width of the incident beam by a factor of K_m (see Eq. 2). For heavy elements like Pt, this effect is small

because K_m is near 1, but for light elements this effect significantly complicates interpretation of the data.

The last two effects are annoying when interpreting measurements on light elements. However, these effects can be minimized by preparing targets with heavy energy markers at the front and rear of the film to be measured. These markers act as near transparent mirrors which reflect projectiles at the surface and at the rear edge of the film. Particles which scatter from the heavy marker lose little energy, hence the incoming and outgoing path are in adjacent energy ranges and one can use an average energy when discussing the energy dependence of straggling. Furthermore, scattering from heavy elements does not modify the energy profile appreciably, so only a small correction is necessary. Appropriate target design can therefore overcome the main disadvantages of using backscattering to measure straggling.

EXPERIMENTAL PROCEDURE

Comparison of Transmission and Backscattering Techniques

Traditionally, straggling has been measured by transmission experiments similar to the idealized experiment described previously. The major disadvantage to this type of experiment is that self-supporting targets are necessary. Uniform, self-supporting films, thin enough for straggling experiments in the energy regime desired, are very difficult to manufacture and to handle. Straggling measurements performed in backscattering, on the other hand, do not require self-supporting targets. Targets can be made by depositing the element of interest on a rigid substrate and this makes them easy to handle.

Target Preparation

The substrate must be chosen so that backscattered signals from it do not interfere with the signal from the film being investigated. For this reason, carbon was used when the films were under investigation for contamination with light elements such as oxygen and nitrogen. For reliable straggling measurements, polished carbon was found to be too rough a substrate, so silicon or silicon dioxide was used throughout.

All targets were prepared by deposition of the element onto clean polished substrates. The Pt targets were RF sputtered using high purity argon as the sputtering gas onto substrates of thermally grown SiO_2. Thickness of the Pt targets was determined gravimetrically.

Targets of the Ni, Au, and Al were prepared by electron beam evaporation at pressures less than 3 x 10^{-6}Torr on a variety of substrates including carbon, SiO_2, and Si. The thickness of these targets was measured by using multiple reflection interferometry.

The Ni and Al samples were prepared with energy markers on Si substrates. Very thin layers of Au were used for the markers in the Al samples. These thin layers were electron beam deposited before and after the deposition of the Al film. Pt was used as the marker material for the Ni samples. For these samples, unlike the Al samples, the low energy marker, i.e., the one deposited between the film and substrate, was heated to form a thin layer of $PtSi_2$ with the Si substrate, before the Ni film was deposited. This was done to prevent the Ni and Pt from mixing due to heating during the Ni deposition. The high energy marker was prepared in the normal way. For a complete discussion of marker thickness and suitability, see Appendix II, p. 72.

Accuracy

Straggling measurements must be freed of spurious effects in order to be trusted. These effects normally enter into the measurement in such a way that the straggling value appears to be inflated. Often, these effects are undetectable by backscattering. This makes identification of erroneous data difficult. Since erroneous straggling measurements are generally larger than the true value, one aims at obtaining straggling measurements which are as low as possible.

The total energy resolution of the system, including the energy width of the incident beam, is always of the same order as the exit profile width. Since the straggling is the root of the difference of the

square of these numbers, small uncertainties in these numbers manifest themselves as a large uncertainty in the straggling data. This difficulty is avoided only when the energy resolution is small compared to the straggling. Two methods for doing this are, first, to measure straggling in films thick enough so that the straggling is large compared to the total resolution. However, this has a limit, because for very thick targets the measurements combine straggling over a large energy range and the energy dependence of straggling becomes difficult to ascertain. The second way is to use high resolution detector systems. The solid state detector system used was limited by the detector to about 15 keV resolution at 2.0 MeV. Magnetic and electrostatic analyzers have much higher resolutions, but they require excessively long measuring times which in turn require a large total dose of particles, and this can damage the target. Typically, one is led to a compromise involving the accuracy of the measurement, the length of time necessary to perform the measurement, and the thickness of the target.

Drift and fluctuations in the incident energy or in any of the electronic system over the measuring time mimics poor resolution, because these effects smear out the measured profile. One must be constantly alert to such effects, or else the work expended in obtaining high resolution is for nought. The methods used to check stability of the backscattering apparatus are discussed in Appendix II, p. 72. These methods, for the most part, involve careful monitoring of the spectra taken on different targets over a period of time and looking for time-dependent changes.

Many of the spurious effects which can enter the measurements originate from the target. Lateral nonuniformity, surface roughness,

and nonuniform density all tend to broaden the exit beam profile and hence tend to make the straggling measurements larger than the actual value. The metals used are believed to have uniform bulk density for films thicker than about 1000Å [27]. Furthermore, the density of the Pt films was checked gravimetrically and found to be bulk density to within about 2%. Investigations of lateral uniformity and surface roughness are described in Appendix II, p. 72, and employ the use of the SEM and Tally Step. Contamination of the films by other elements can also invalidate straggling measurements. The purity of the targets was checked by preparing films on C substrates and determining the contamination level by backscattering. The only appreciable contamination found was that of oxygen in the Al targets at a level of about 2 atomic percent. The significance of this is discussed in Appendix II, p. 72.

The number of counts in a channel is a statistical quantity which obeys Poisson statistics. Hence, determination of the width of either the incident beam profile or the exit beam profile is subject to the uncertainties in the number of counts in the channels of interest. This statistical error prevents one from obtaining these energy differences to much better than ±1 channel or ±2 keV.

Considering the uncertainties introduced by the target, the backscattering apparatus and the evaluation from the spectra, the straggling values presented here have an overall uncertainty of about 10%. The various statistical and systemic errors in these measurements are discussed in Appendices I, p. 64 and II, p. 76.

RESULTS

Discussion

The energy distribution for particles traversing a thin absorber is in general a skewed, bell-shaped function. The transport equation describing the energy loss of heavy charged particles in thin targets has been solved rigorously by Vavilov[28]. The Vavilov distribution has two limiting forms. In the limit that the maximum possible energy which can be lost by the projectile to an atomic electron is large compared to the total energy lost while traversing the absorber, the Vavilov distribution approaches the Landau distribution [29]. If the maximum possible energy which can be lost to an atomic electron is small compared to the total energy lost, the Vavilov distribution approaches a Gaussian. The latter case closely approximates ^{4}He at 2.0 MeV penetrating targets from 1000 to 4000Å thick. In Vavilov's derivation he assumed that the cross section for collisions between projectiles and atomic electrons was constant over the projectile's path. This approximation is valid so long as the energy lost in traversing the target is small compared to the incident energy, which is the case for the thin films studied here. If, on the other hand, the films are thick and an appreciable fraction of the incident energy is lost during target penetration, Tschalar's [30] modification of Vavilov's theory must be used.

The exit beam energy profile for Pt, Ni, Au and Al targets in the energy and thickness range considered is approximately a Gaussian (see Appendix II, Fig. 2, p. 71.) The energy straggling is proportional to the square root of thickness. This is consistent with the

predictions of Bohr's theory[31] which gives

$$\Omega_B^2 = 4\pi z_1^2 e^4 z_2 N \Delta R$$

where

Ω_B = the straggling (standard deviation)

z_1 = atomic number of projectile

z_2 = atomic number of target atoms

N = atomic density

ΔR = projectile path length.

Bohr's theory assumes that (i) the target atoms are randomly distributed, (ii) the velocity of the projectile is high compared to the orbital electron velocities, (iii) the cross section for electronic collisions is constant over the projectile's path. Assumption (ii) is violated even for 2 MeV ^{4}He particles penetrating Al. The reverse assumption is actually more applicable for inner shell electrons of elements like Au. Therefore, it is not surprising that Bohr's theory disagrees with the measurements by as much as 40% in Au. Figure 3 shows a plot of straggling vs. square root of target thickness for Al, Ni, Pt and Au. Bohr's theory applied to energy straggling in the back-scattering configuration in these targets is also given.

The theory of Lindhard and Scharff [15]modifies Bohr's theory when condition (ii) is not applicable. Even though the approach of L&S is to treat the target as an electron gas using the Thomas-Fermi model of the atom, the result of the derivation is to modify the electron density ($NZ_2\Delta R$) in Bohr's formula to account for the interaction

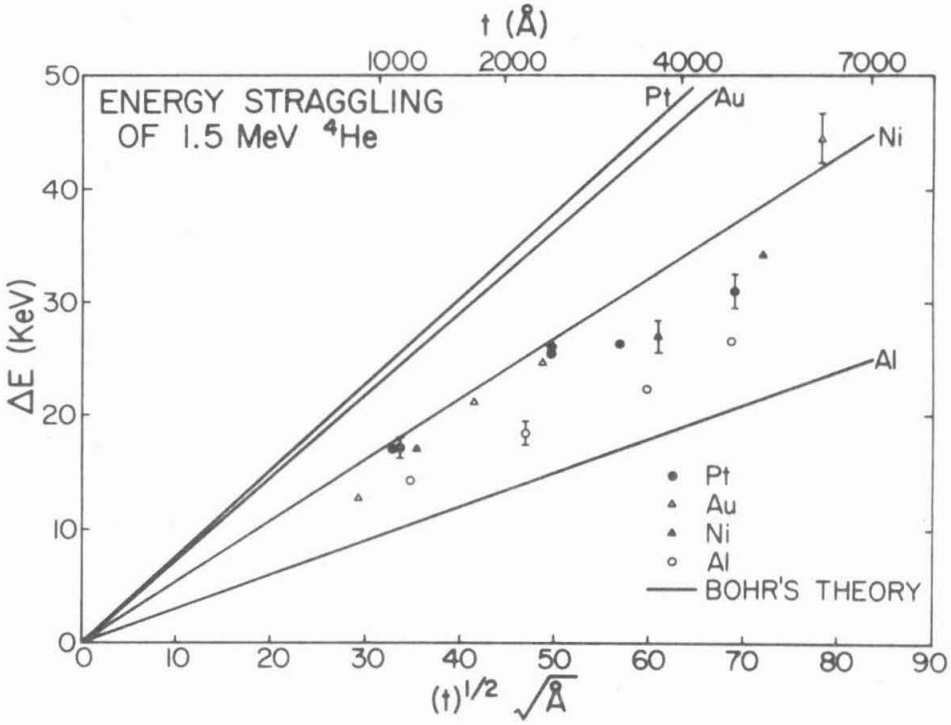

Fig. 3. Energy straggling ΔE (FWHM) of ^{4}He ions at 1.5 MeV incident energy in Al, Ni, Pt and Au vs. the square root of target thickness. Bohr's theory calculated for B.S. configuration.

of the projectile and the more tightly bound of the atomic electrons. The L&S theory gives

$$\Omega^2_{L\&S} = \Omega^2_B \begin{cases} L(\omega)/2 & \text{for } \omega \leq 3 \\ 1 & \text{for } \omega > 3 \end{cases} \qquad (14)$$

where $\omega \equiv z_2 v^2/v_o^2$

v = velocity of the projectile

v_o = velocity of first Bohr electron = $e^2/\hbar = 2.19 \times 10^8$ cm/s

and $L(\omega)$ is the stopping number. $L(\omega)$ can be calculated from

dE/dx by

$$\frac{dE}{dx} = \frac{4\pi z_1^2 e^4}{mv^2} N z_2 L(\omega) \qquad (15)$$

or approximated by

$$L(\omega) = 1.36\ \omega^{1/2} - 0.016\ \omega^{3/2} \qquad (16)$$

Chu and Mayer [20] have taken the correction of Bohr's formula one step further by using a more realistic expression for the atomic electron density, namely that calculated from Hartree-Fock-Slater wavefunctions in the formalism of Bonderup and Hvelplund [37]. Both the calculations of L&S and C&M asymptotically approach Bohr's theory at high projectile velocity ($\omega \geq 3$ corresponding to about 4 MeV for He in Al and 24 MeV for He in Au.) The C&M calculation displays z_2 oscillations similar to those obtained in dE/dx calculations using Hartree-Fock-Slater wavefunctions [16]. The predictions of L&S and C&M both underestimate the experimental results by about 20% for Au, Pt and Ni.

The energy dependence of straggling is very weak, see Fig. 4, but the data is so rough that a more precise statement is difficult. It is not clear which of the theories best describes the energy dependence of the data. However, the theories of C&M and L&S seem to fit somewhat better for all the elements except Al than does Bohr's theory, which predicts no dependence of straggling on energy. (See Appendix I, Fig. 2, p. 65 , and Appendix II, Fig. 6, p. 75.)

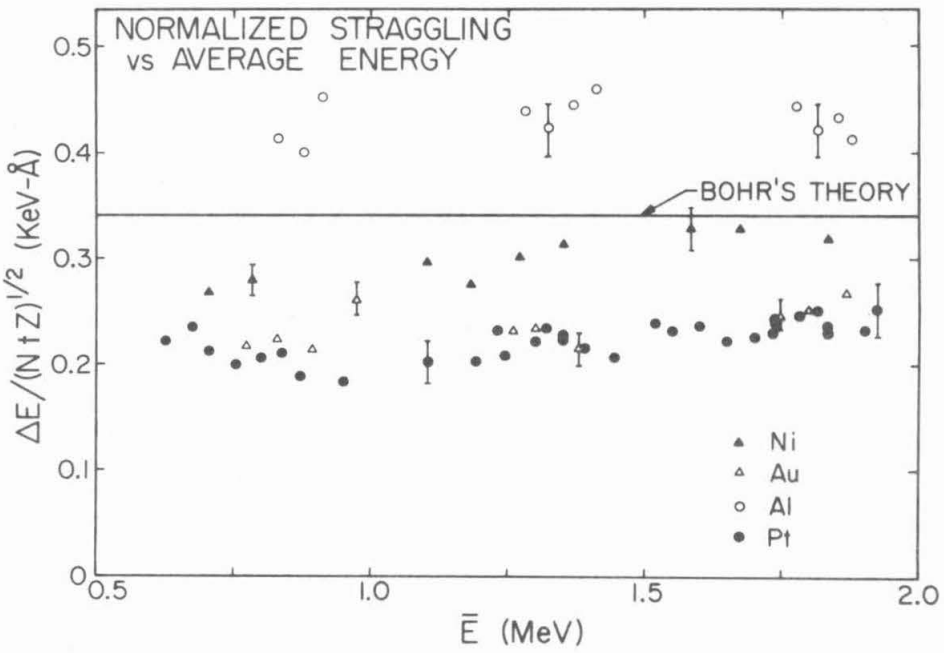

Fig 4

Fig. 4. Normalized energy straggling as a function of average energy in targets of Al, Ni, Pt, and Au vs. average energy in the target.

The experimental straggling for Al seems anomalously high with respect to theory, approximately 30% higher than Bohr's theory. Demichelis [32] has measured the energy straggling of ^{4}He in Al at incident energy of about 5.3 MeV for targets ranging in thickness from about .4 μm to 8 μm. For the thinner targets the measurements were about 75% higher than Bohr's theory and Demichelis concludes, "In aluminum the straggling is not measurable because of the irregularity of the foils." Measurements of ^{4}He straggling in Al by Sykes and Harris [33] at an incident energy of

5.49 MeV are consistent with those of Demichelis for comparable absorber thicknesses, and again the authors comment, "The accuracy of the technique was limited by the difficulty in obtaining very thin uniform absorbers...". The measurements presented here are not strictly comparable with the two previous sets of measurements, since the previous measurements were at higher energies and in thicker absorbers. However, the accuracy of the present data may also be limited in part by the quality of the targets. Even so, the experimental values given here place an upper bound on straggling which is lower than the one obtained by extrapolating the previous measurements to thin films. It would be interesting to make measurements in thin films at the higher energies to see if they merge with the thick film measurements.

Previous measurements of ^{4}He straggling in the remaining elements are all at higher energy and in thick absorbers. The measurements of Comfort et al. [34] in Ni at an incident energy of 8.7 MeV are slightly above Bohr's theory for the thinnest targets which are about a micron thick. Comfort also measured straggling in Au and Al. In Au absorbers, also a micron thick, the data are about 40% above Bohr's prediction. Comfort's aluminum data are similar to both sets of measurements mentioned earlier, in that for the thinnest absorbers the experimental values are almost a factor of two above Bohr's predictions.

Comparisons can be made between data for the straggling of ^{1}H and ^{4}He in the various materials. Since straggling is proportional to z_2, $^{4}He^{++}$ straggling is expected to be twice the straggling of $^{1}H^{+}$, other parameters held equal. Furthermore, one should compare data for which the projectile velocities are equal; hence, 2.0 MeV ^{4}He straggling data

are comparable with 0.5 MeV ^{1}H straggling data. Measurements of ^{1}H straggling in Au near 0.5 MeV by Madsen [26] are about 30% below Bohr's theory. This is consistent with the data given here. Furthermore, proton straggling measurements in Co, Fe [35] and Ni [36] roughly agree with Bohr, similar to the present measurements. The proton straggling measurements made in Al [26] agree roughly with Bohr also, whereas the present data are about 30% high.

Conclusion

Straggling measurements of ^{4}He in Al, Ni, Au and Pt below 2.0 MeV have been made. The results are qualitatively described by a very simple theory, namely that of Bohr. Quantitative agreement is not very good for any of the theories presented. The Al data are above Bohr's theory but lower than extrapolations made from previous ^{4}He straggling measurements. The Ni results are closest to Bohr's predictions. The Au and Pt data are very close to one another and between 30% and 40% below Bohr's theory. The ^{4}He straggling is roughly consistent with ^{1}H straggling data, except for the measurements made in Al, where the ^{4}He measurements are somewhat high.

REFERENCES

Part I

1. H. Geiger and E. Marsden, Proc. Roy. Soc. (London) A82, 495 (1909).

2. S. Rubin, T. O. Passell, and L. E. Bailey, "Chemical Analysis of Surfaces by Nuclear Methods", Anal. Chem. 29, 736 (1957).

3. A. L. Turkevich, et al, "Surveyor Project Final Report I: Part 2, Science Results", Jet Propulsion Lab. Tech. Report No. 32-1267 (15 June 1968), p. 303.

4. M-A. Nicolet, J. W. Mayer, I. V. Mitchell, Science 177, 841 (1972); W. D. Mackintosh, "Rutherford Analysis" in Characterization of Solid Surfaces, ed. Kane and Larrabee (Plenum Press, New York, 1974), Ch. 16; W.K. Chu, et al., Thin Solid Films 19 (1973) p.430.

5. D. J. Ball, T. M. Buck, and G. H. Wheatley, "Studies of Solid Surfaces with 100 keV He^+ and H^+ Ion Beams", Surface Science 30, 69 (1972); J. M. Harris, E. Lugujjo, S. U. Campisano, and M-A. Nicolet, "Studies on the Al_2O_5-Ti-Mo-Au Metallization System", J. Vacuum Sc. and Tech., Jan.-Feb. issue (1975).

6. R. D. Evans, The Atomic Nucleus (McGraw-Hill Book Company, New York, 1955), p. 828, Appendix B.

7. H. Bethe, Ann. Physik 5, 325 (1930); F. Bloch, Ann. Physik 5, 285 (1933).

8. U. Fano, Ann. Rev. Nucl. Sci. 13, 1 (1963).

9. W. H. Barkas and M. J. Berger, Studies in Penetration of Charged Particles in Matter, National Acad. Sci.--National Res. Council Publ. No. 1133, 1964, p. 103.

10. M. C. Walske, Phys. Rev. 88, 1285 (1952); M. C. Walske, Phys. Rev. 101, 940 (1956).

11. H. Bichsel, Tech. Report No. 3, Physics Dept., University of Southern California (June 21, 1961) and Appendix.

12. U. Fano and J. E. Turner, p. 49 of Ref. 8.

13. R. M. Sternheimer, Phys. Rev. 103, 511 (1956); R. M. Sternheimer Phys. Rev. 145, 247 (1966).

14. A. Brynjolfsson, Doctoral Thesis, University of Copenhagen, 1973.

15. J. Lindhard and M. Scharff, Dan. Mat. Fys. Medd. 27, 1 (1953).

16. J. F. Ziegler and W. K. Chu, IBM Research Report R.C. 4288, (1973); also, Thin Solid Films 19, 281 (1973).

17. J. Lindhard and A. Winther, Kgl. Danske Videnskab. Selskab, Mat.-Fys. Medd. 35, No. 17 (1967).

18. D. K. Brice, Phys. Rev. A 6, 1791 (1972).

19. O. B. Firsov, Sov. Phys. JETP 36, 1076 (1959).

20. Catania Working Data for Ion Beam Analysis, ed. J. Mayer and E. Rimini, June 1974.

21. L. C. Northcliffe and R. F. Schilling, Nuclear Data Tables, Academic Press, New York, Section A, Vol. 7, No. 3-4, 1970; p. 233ff; Williamson, Boujot, Picard, Report CEA-R 3042 (1966), J. F. Janni Air Force Weapons Lab, Report AFWL-TR-65-150 (1966); H. Bichsel, Am. Inst. of Physics Handbook, McGraw Hill, New York, 1963, p. 8ff. Also, Ref. 8.

22. W. A. Wenzel, Ph.D. Thesis, California Institute of Technology, 1952; D. Powers and W. Whaling, Phys. Rev. 126, 61 (1962).

23. R. Behrisch and B.M.U. Scherzer, Thin Solid Films 19, 250 (1973).

24. A. van Wijngaarden, E. J. Brimner, and W. E. Baylis, Canadian J. of Physics 48, 1835 (1970); F. T. Smith, Phys. Rev. 161, 31 (1967).

25. J. R. Cameron, Phys. Rev. 90, 839 (1953).

26. C. B. Madsen and P. Venkatesworlu, Phys. Rev. 74, 1782 (1948); C. B. Madsen, K. Dan Vidensk. Selsk. Mat.-Fys. Medd. 27, 13 (1953).

27. K.N. Tu. Private communication.

28. P. V. Vavilov, Zh. Exper. Teor. Fiz. 32, 320 (1957). Transl. JETP 5, 749 (1957).

29. L. Landau, J. Exp. Phys. (USSR) 8, 201 (1944).

30. C. Tschalar, Nuclear Instr. and Methods 61, 141 (1968).

31. N. Bohr, Mat. Fys. Medd. Dan. Vid. Selsk. 18, No. 8 (1948).

32. F. Demichelis, I.L.Nuovo Cim. 8, 2134 (1959).

33. D. A. Sykes and S. J. Harris, Nuclear Instr. and Methods 94, 39 (1971).

34. J. R. Comfort, J. F. Decker, E. T. Lynk, M. O. Scully and A. R. Quinton, Phys. Rev. 150, 249 (1966).

35. E. Leminen and A. Anhila, Ann. Acad. Sci. Fenn. A6, No. 370 (1971).

36. L. P. Nielsen, K. Dan Vidensk. Selsk. Mat.-Fys. Medd. 33, No. 6 (1961).

37. E. Bonderup and P. Hvelplund, Phys. Rev. A 4 No. 2 1971, p.562.

38. J. Lindhard, V. Nielsen and M. Scharff, K. Dan Vidensk. Selsk. Mat.-Fys. Medd. 36, 10 1968; W. White and R.M. Mueller, Phys. Rev. 187 No. 2 p.499 1969.

PART II

STUDIES OF THE Ti-W METALLIZATION SYSTEM ON Si

Part II

INTRODUCTION

Interaction of Ti-W with Si

Titanium and tungsten have both been used for many years as materials for metallizing integrated circuits [1]. Tungsten is used because its coefficient of expansion closely matches that of silicon near process temperature (at 400°C $\alpha_{si} = 4.1 \times 10^{-6}$ ($°C^{-1}$) and $\alpha_{W} = 4.7 \times 10^{-6}$ ($°C^{-1}$)) and titanium is used because of its strong adherence to oxides. A metallization scheme has also been developed which uses a mixture of titanium and tungsten [2]. Like many of the transition materials, Ti and W both form silicides. The formation of WSi_2 from thin tungsten films on Si has been studied by several authors [3,4]. The formation of $TiSi_2$ from thin films on Si has also been studied [5], although not to as great an extent as WSi_2. To our knowledge, the present investigation is the first to consider the interaction of a mixed thin film with silicon. This study shows that, like Ti and W individually, a thin composite layer of Ti and W, deposited on Si by sputtering and annealing in vacuum, forms a disilicide. This ternary disilicide was studied using the techniques of X-ray diffraction, ^4He backscattering spectrometry (BS) and Auger electron spectrometry (AES).

Interaction of Au with Ti-W

Au is used as the final layer for many of the industrial metallization schemes involving Ti-W. It is therefore important to investigate the interaction of Au with Ti-W. The Ti-W layer should prevent the Au from contacting the Si substrate, otherwise Au may enter the Si and alter device characteristics. However, samples prepared from Au

deposited on sputtered Ti-W films on Si and annealed in vacuum from 20 min to 1 hr at temperatures from 350 to 400°C revealed that Au and Si had intermixed. These samples were studied using a SEM and Electron Microprobe (EMP).

SAMPLE PREPARATION

Films of 1000 to 1500Å were deposited by RF sputtering from an arc-melted $Ti_{0.3}W_{0.7}$ target onto silicon and carbon substrates. The silicon substrates were n- or p-type 1 to 10 Ω-cm single crystal wafers of <111> , <110> or <100> orientations which had been mechanically polished and chemically etched. The polycrystalline carbon substrates were 0.5 in. squares and were polished and cleaned prior to sputter-deposition.

During deposition, the substrates rested on a cooled copper pallet and the deposition temperature was monitored by a shielded iron-constantan thermocouple placed on the substrate surface. Substrates were loaded through a side loader which was evacuated by a cryogenic pumping station so as to prevent contamination of the target during loading.

Prior to loading, the silicon substrates were dipped in HF, rinsed in deionized water and dried with high purity isopropanol. After loading, the sputtering chamber was evacuated to a background pressure of 1×10^{-6} Torr. Argon of 5N purity which had passed through a titanium purifier was used to backfill the chamber. The Ti-W target was given a short presputter to insure a clean surface, and the substrates were sputter-cleaned immediately before deposition.

During deposition the substrates were held at a negative bias ranging from 0 to -50 volts with respect to ground. The maximum temperature measured during deposition was about 300°C. The Ti-W film deposited on Si has a resistivity of about 80 μΩ-cm, irrespective of the substrates or bias voltage. The films deposited on carbon were analyzed by BS to check for possible contaminants. No oxygen or nitrogen could be detected. The samples deposited with -50V bias showed the largest amount of contamination, which consisted of Ar and was less than 2 atomic percent (at.%). Examination of the film on silicon substrates by SEM at 30K magnification revealed a featureless surface.

Samples were also prepared with Au layers sputter-deposited immediately following the Ti-W deposition without breaking vacuum. Substrates were of <111> orientation only and depositions were made with both 0 and -50V substrate bias. The resistivity of the Au layers was near bulk regardless of substrate bias. Examination of the samples by SEM at 30K magnification revealed a featureless surface.

Annealing was performed in an evacuated quartz-tube furnace. The furnace was pumped from one end by a LN_2 trapped oil diffusion pump and from the other end by a water cooled titanium sublimation pump. The vacuum during annealing was typically 7×10^{-7} Torr. The temperature in the center of the furnace was measured by a chromel alumel thermocouple which had been calibrated to an accuracy of ±1°C against a mercury thermometer to a temperature of 350°. The thermometer was calibrated against the freezing point and the boiling

point (corrected for barometric pressure) of H_2O. The temperature stability of the furnace was measured to be ±2° over a period of 20 hr. The furnace was constructed so that many samples could be loaded and annealed sequentially during a single pump-down, and samples were always placed at the position within the furnace where it had been calibrated. Samples could be grouped and annealed simultaneously in the furnace.

ANALYTICAL TECHNIQUES

Backscattering Spectrometry (BS)

The experimental setup and analytical method for BS have been reviewed elsewhere [6]. In brief, the technique consists of placing a sample in a beam of monoenergetic $^4He^+$ ions and energy analyzing those He atoms which are scattered from the sample. BS with MeV $^4He^+$ ions provides information on concentration profiles in depth with a resolution of about 200Å and to depths of about 3000 to 5000Å. In thicker films, the depth resolution degrades due to energy straggling within the target. The beam spot is typically 1 to 2 mm^2 and hence backscattering analysis requires samples whose lateral composition is uniform over at least such a dimension.

X-Ray Analysis

Two types of X-ray diffraction analyses were performed. The first type uses the Reed Camera [7] geometry which is basically a glancing angle X-ray diffraction setup with a fixed angle of incidence. The structure of the thin-film samples is identified in a manner similar to that employed with the Debye-Scherrer camera. Because of the glancing angle of incidence of the X-rays (8 to 14° with respect to the specimen surface), a relatively large volume is examined although the samples are thin. For example, at a incident angle of 10° the X-ray path length is 6 times the film thickness. The incident X-ray beam used for the exposure was CuK_α radiation collimated through two pin holes. The diffraction pattern is recorded on film placed along a 5 cm radius from the sample center.

The second type of X-ray diffraction analysis performed, used a Guinier camera [8]. This is a transmission X-ray diffraction apparatus in which the sample rotates with respect to the beam during exposure. CuKα radiation was used in conjunction with X-ray film to record the diffraction patterns. The Guinier camera requires thin samples so as to not substantially attenuate the diffracted X-rays. To this end, the rear side of a reacted sample was lapped until the sample thickness was reduced to between 50 and 60 microns. The sample was then ultrasonically cleaned and rinsed in dilute HF. A similar sample of the bare silicon substrate was also prepared in this way. By comparing the X-ray diffraction patterns from both samples, the diffraction lines due to the silicide could be identified.

Given the camera constant and an accurate measurement of the silicide diffraction line spacing, determination of the cell parameters can be made. The camera constant was determined by measurement of the camera radius and verified using the diffraction lines from a strain-free sample of polycrystalline silicon powder. The silicide diffraction line spacing was measured with an optical comparator to ±.01 mm, which gave an uncertainty of ±.01Å in the cell constants. The advantage of the Guinier technique is to enable an accurate determination of the cell constants, whereas the Reed camera can detect the presence of phases without special preparation of specimens.

Auger Electron Spectroscopy (AES)

AES has been reviewed recently in the literature[9]. This technique uses the decay by electron emission of sample atoms which experience inner shell ionization by an energetic electron beam. Energy

analysis of these emitted Auger electrons allows one to perform an elemental analysis of the sample surface. Typically, sensitivities of about 1 at.% can be obtained.

Auger electrons originate only from atoms excited in the outermost atomic layers. Hence, elemental depth profiling requires a sequential removal of thin layers between measurements. This can be accomplished by sputtering. To obtain the depth profile of a sample requires knowledge of the sample's sputtering rate and the sputtering time. BS can be used conveniently to determine the film thickness and thereby calibrate the sputtering rate.

AES and BS nicely compliment each other. AES is more sensitive than BS for profiling light elements in heavy matrices, and BS can be used to measure the thickness and composition of the film quantitatively in a relatively short time ($\sim$ 10 to 20 min).

RESULTS

Characterization of Ternary Silicide

Films of Ti-W having about 30 at.% Ti (10% by weight), prepared as described above, were vacuum annealed at 800°C for 20 min. The surface changed from the shiny metallic luster of Ti-W to a deep silver-gray. Examination by SEM at 4500 X magnification revealed a uniform and gently undulating surface. The undulations were typically 2.5μ across and < .05μ in height (measured using a Sloan Dektak).

X-ray diffraction analysis by Reed camera revealed the presence of only one compound (Figure 1). The diffraction pattern corresponds to that described by the ASTM powder diffraction compilation No. 6-0599 [16]. This compound has a chemical formula of $Ti_xW_ySi_2$, where $x + y = 1$, with a hexagonal $CrSi_2$-type (C-40) structure. X-ray analysis by the Guinier camera supported the Reed camera results in that no crystal structures other than the C-40 type were detectable. The line spacings from the Guinier photographs gave cell parameters of $a_o = 4.61 \pm .01\text{Å}$ and $c_o = 6.48 \pm .01\text{Å}$.

Once formed, the compound adheres strongly to the silicon substrate. The compound seems unaffected by hot H_2O_2, HF or CP-4 [17] and dissolves only slowly in aqua regia. Indium solder would not adhere to the compound.

Analysis of films reacted at 725°C for 40 min by 2 MeV ^4He BS revealed that the atomic concentration ratio of the films is Ti:W:Si = 0.30:0.7:2.0 (see Fig. 2). The compound maintains this composition at

temperatures ranging from 675°C to 900°C. Additional experiments established that the compound formed was independent of substrate orientation, doping type, substrate bias during sputter deposition, and the sample contamination by oxygen during annealing.

Fig. 1. X-ray diffraction pattern taken with Reed Camera (top), and Guinier Camera (bottom) of reacted samples.

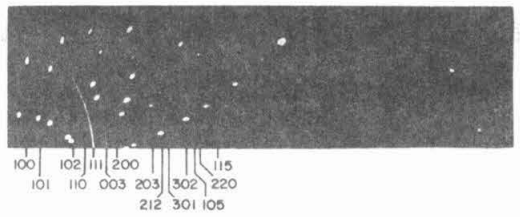

Read camera x-ray diffraction pattern of a sample after heat treating at 800°C for 20 minutes showing the presence of $Ti_x W_y Si_2$, where $x+y=1$. Some of the diffraction rings are labeled. The x-ray incident angle is 12°. Cu K_α radiation was used.

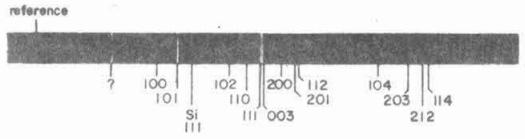

Guinier x-ray diffraction spectrum of sample annealed 750°C 1 hr showing $Ti_x W_y Si_2$ on Si substrate. Structure is hexagonal with a = 4.61Å c = 6.48 Å. Radiation was Cu, $\lambda = 1.54178$ and camera constant = .35810. The unindexed line was also present in diffraction spectrum taken of Si substrate.

Kinetics of Silicide Formation

The reaction rate of the compound formation was investigated by BS on samples annealed in vacuum for increasing periods of time. To translate the energy scale of a BS spectrum into a depth scale, we assumed a density of 7.54×10^{22} atom/cm^3 for the compound, as calculated from the measured unit cell parameters. Using this density, 10 keV in a BS spectrum corresponds to about 106Å of compound.

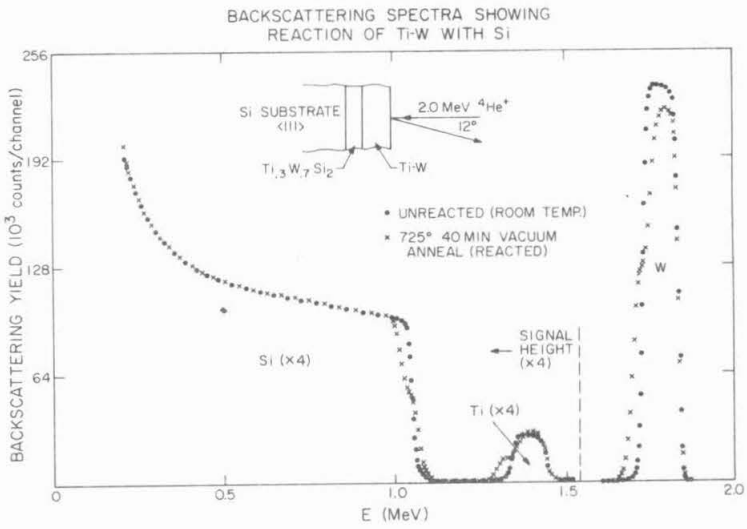

Fig. 2. Backscattering spectra of a virgin (room temperature) sample of Ti-W on Si and a sample covered during annealing ($725^{o}C$, 40 min, 7×10^{-7} Torr). The Si substrate is <111> single crystal n-type with resistivity of 10Ω-cm. The Ti-W film was deposited with -50V bias.

Films deposited on <111> silicon at -50V bias and annealed at 5×10^{-6}Torr and 725°C were found to have reaction rates of about 9.7Å/min. Improving the vacuum to 7×10^{-7}Torr and covering the metallized side of the sample with a clean Si wafer during annealing increased the reaction rate by approximately a factor of 2 (see Figure 6). Figure 3 shows a BS spectrum of a <111> silicon sample of which half of the metallized side was covered with a Si wafer during annealing at 7×10^{-7} Torr and $725^{o}C$ for 45 min. The uncovered side (top) shows little reaction whereas the covered side (bottom) is almost completely reacted. A subsequent AES analysis of this sample (Figure 4) reveals that the uncovered half of the sample has a larger concentration of oxygen than does the covered half.

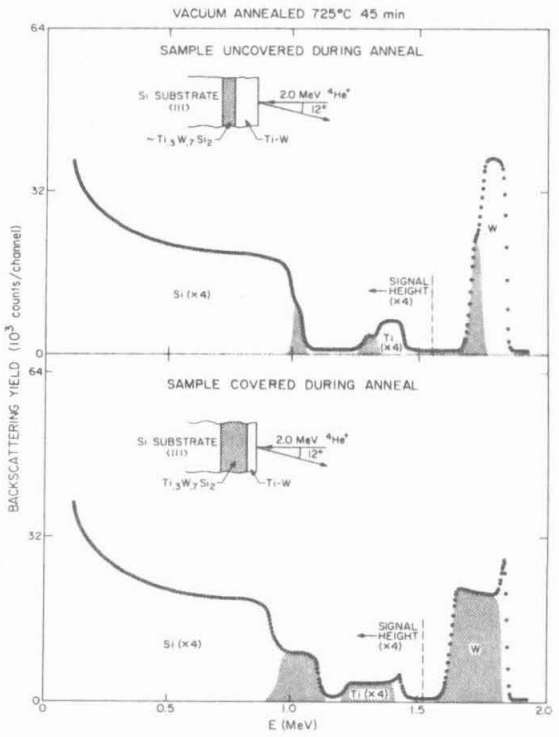

Fig. 3. Backscattering spectra of a partially covered sample annealed at 725°C for 45 min. (Top) Spectrum for portion of sample which was uncovered during anneal and (bottom) spectrum for covered part.

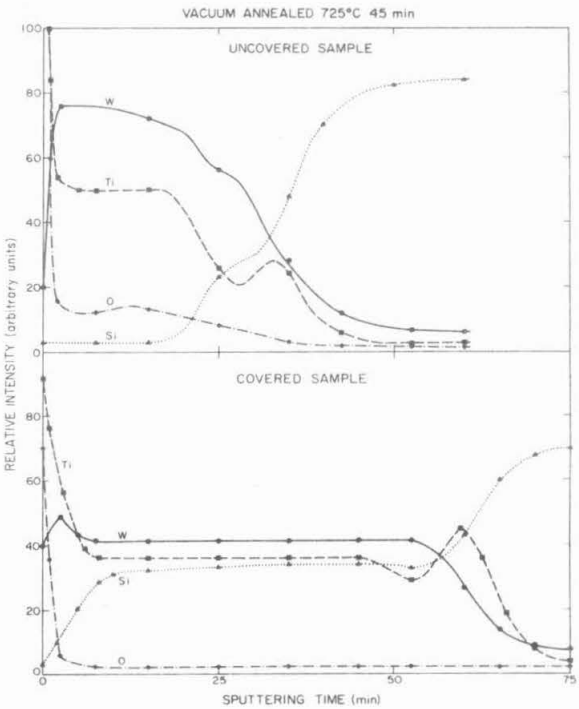

Fig. 4. AES depth profile of W, Ti, Si and O in the uncovered (top) and covered (bottom) parts of the sample in Fig. 3

In Figure 2 the ratio of the signal height of the remaining unreacted tungsten to that of the unreacted silicon substrate is smaller than that same ratio measured on the virgin sample. This was still true for partially reacted samples which had been covered and annealed in the highest vacuum attainable ($\sim 7 \times 10^{-7}$ Torr). If this difference is attributed to oxygen contamination, then the samples annealed in the cleanest vacuum still contained up to 15 at.% oxygen. Since oxygen has been shown to influence rates, the kinetics studies performed here are to be interpreted with caution and the results should be regarded as preliminary.

Reaction rate studies at 750°, 725° and 700°C were performed on covered samples annealed at 7×10^{-7}Torr. Samples annealed at each temperature were all cut from the same wafer and loaded simultaneously. The samples were then annealed sequentially. When precautions to reproduce the vacuum were taken, the results were reproducible. The analysis of the backscattering yields established that after anneal all the samples were contaminated 15% to 20%, presumably by oxygen. The reaction has a linear time dependence at all temperatures and over the entire range of oxygen contamination. An apparent activation energy of 4.5 eV is determined from the reaction rate vs temperature (see Figure 5).

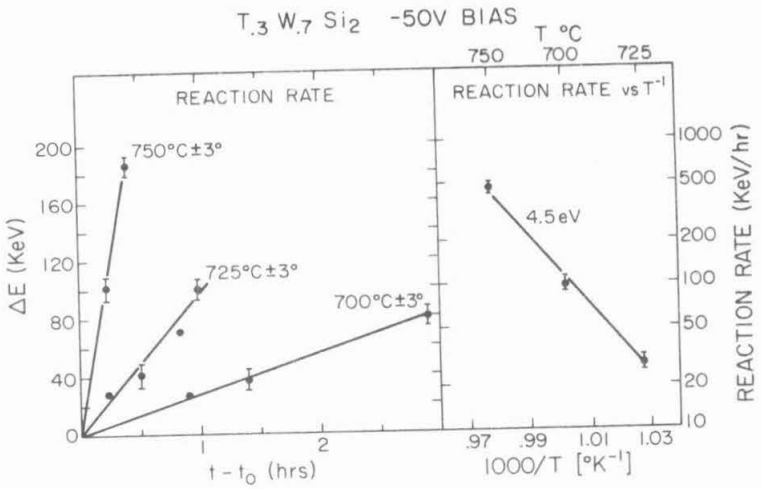

Fig. 5. (Left) plot of compound thickness (expressed in terms of backscattering energy loss for 2.0 MeV $^4He^+$ ions; 10 keV corresponds to about 106Å of compound) vs anneal time, t, minus warm-up time t_o .
(Right) plot of log of reaction rate vs reciprocal annealing temperature (yields activation energy of 4.5 eV).

The rate of reaction is influenced by several parameters. This fact was established by comparing two samples which differed only in the parameter of interest. These sample pairs were sandwiched together with the metallized sides face to face and annealed in a vacuum similar to that used in the rate vs temperature studies. This procedure also gave reproducible results. From such comparison, it was established that the reaction rate is influenced by the bias applied during sputtering deposition (see Figure 6). Samples deposited on <111>-silicon substrates react more slowly than those deposited on <110>, and samples prepared on <100> react fastest. On the other hand, the dopant type of the Si substrate had no measurable effect on the reaction rate, nor did changes of the doping level from 2 to 10 Ωcm.

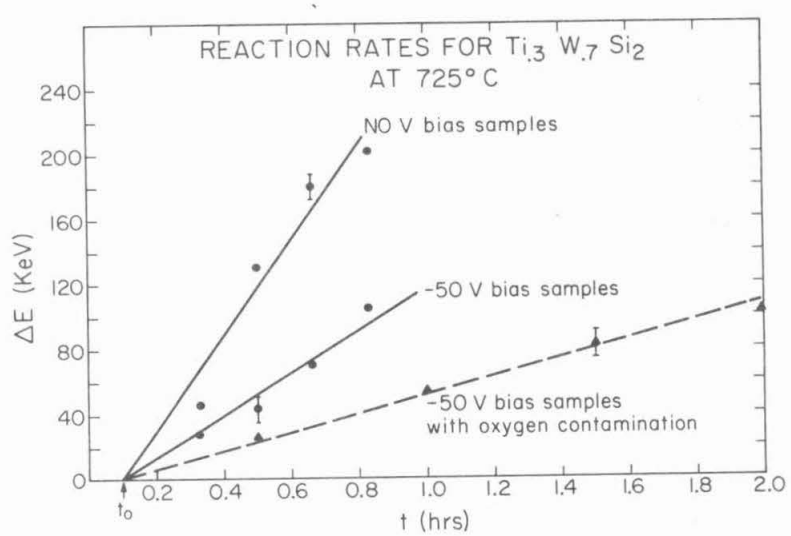

Fig. 6. A plot of compound thickness (expressed in terms of backscattering energy loss) vs annealing time. t_o is the warm-up time for a sample when placed in the vacuum furnace. The lines show the effect of deposition bias and oxygen contamination on reaction rate. (10 keV corresponds to about 106Å of compound).

Interaction of Au on Ti-W

Samples with between 1000Å and 1100Å of Au deposited on Ti-W on <111> Si at -50V substrate bias were vacuum annealed at 400°C for 45 min. The surface changed from yellow gold color to a metallic silver. Examination under an SEM revealed that the surface had fractured into linear fissures approximately 3 μm wide and extending over the entire sample. Microprobe analysis of the fissures indicated that the Au had segregated there and filled them. SEM micrographs of the fissures at 44K magnification showed that the Au filling had numerous triangular holes approximately 0.7 μm on a side. When the Ti-W was etched away the remaining Au formed large ridges and it was evident that Au had collected along the fissures and at the interface between the Ti-W and the Si (see Figure 7). The Si-Au eutectic temperature is at 371°C.

Studies with vacuum anneals at 360°C for up to 1 hr on sample deposited at 0 bias on <111> Si substrates showed similar behavior to those above. However, the samples with 0 bias had fractures which formed polygon-like features (see Figure 8c) rather than the linear features described above. Samples annealed for 21 min had pits and holes approximately 5 μm in diameter which were triangular in nature covering the surface (see Figure 8a). These holes were not present in the 50V samples annealed at 400°C. Each hole had a circular ring approximately 15 μm in diameter around it. Microprobe analysis showed that the area within the ring was depleted of Au and that the interior of the hole was Au rich. Analysis by microprobe on samples annealed

for 46 min at 360° showed that the Au layer had vanished from large areas of the surface. Furthermore, heavy buckling was observed where fissures intersect to form the polygons.

Fracturing and the catastrophic morphological changes described above were also observed on samples annealed at 350°C for 3 hrs.

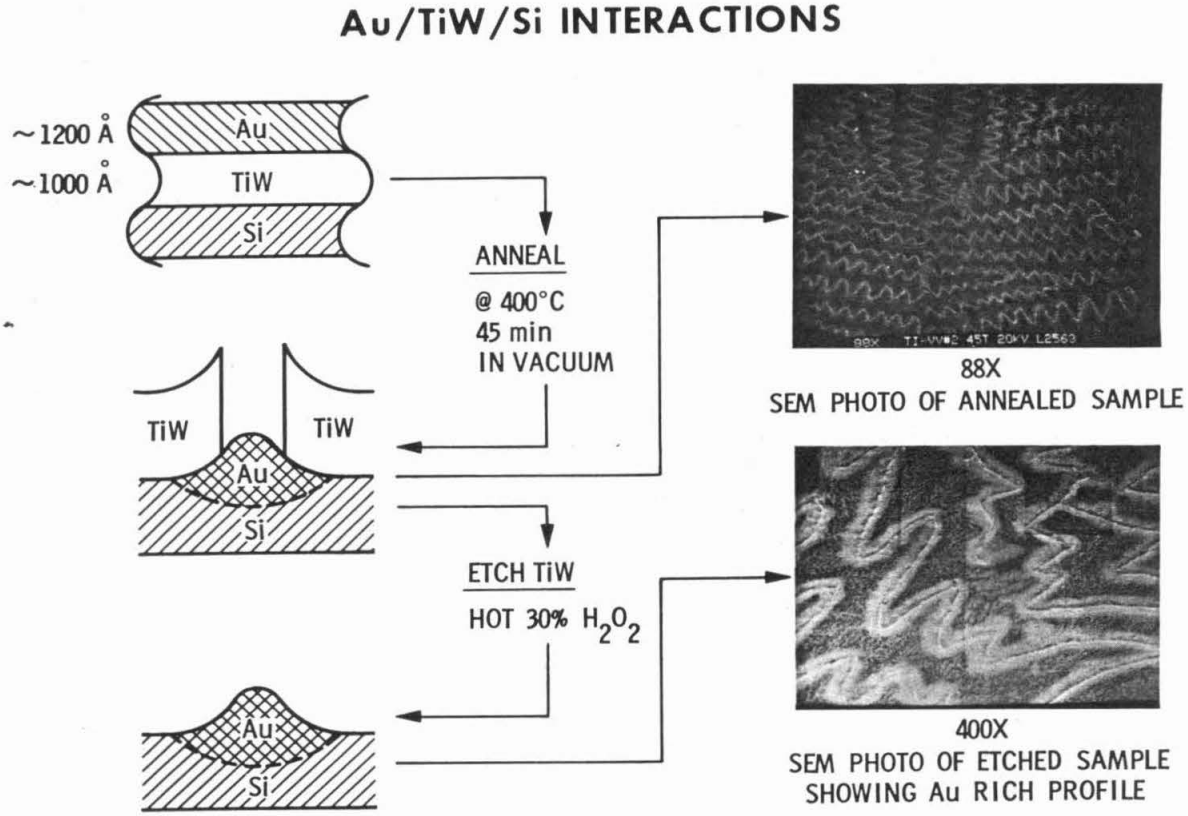

Fig. 7. Au/Ti-W/Si sample annealed in vacuum 45 min at 400°C, showing linear fissures. Sample with TiW removed after annealing exposing the Au rich area.

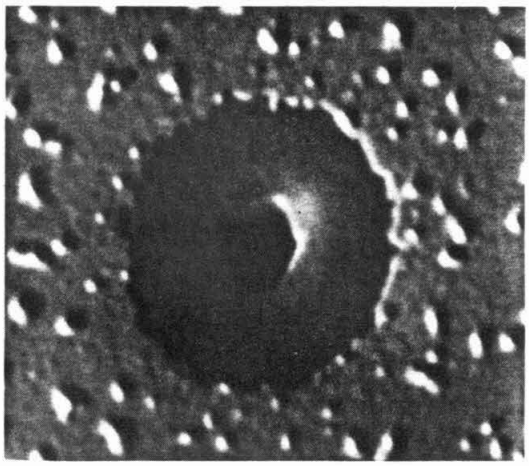

a

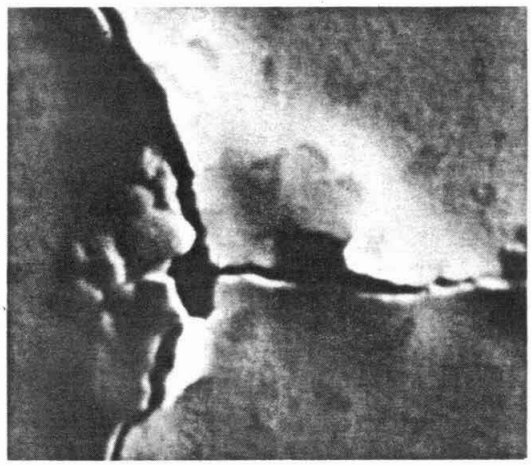

b

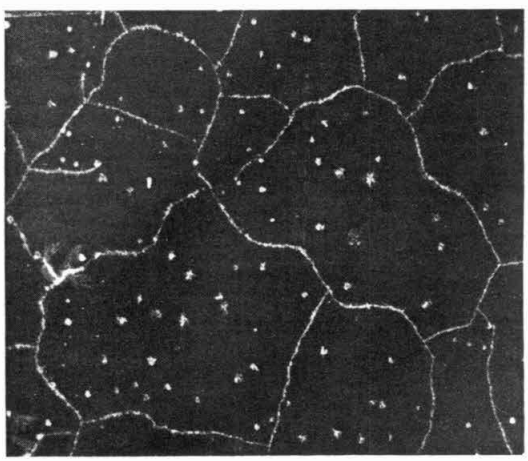

c

Fig. 8. Surface morphology of a $Ti_{0.3}W_{0.7}$-Au bilayer annealed under vacuum at approximately 360°C for (a) 21 min, (b) 46 min, and (c) 63 min. Figure 8a shows a circular area of approximately 15 μm dia. of TiW where the Au layer is missing, and with a hole at the center whose contour reveals the 3-fold symmetry of the underlying Si (111) substrate. In Fig. 8b (same magnification as for 8a) the Au layer has vanished and the TiW layer has fractures which extend over the whole surface as shown in Fig. 8c (magnification is 30 times less than in Figs. 8a and b). (Samples with 0V bias during deposition).

V. DISCUSSION AND CONCLUSION

Interaction of Ti-W and Si

Ternary disilicide like $Ti_{0.3}W_{0.7}Si_2$ can be thought of as a compound formed from two binary disilicides. In the present case the binary compounds are $TiSi_2$ and WSi_2. Typically with transition metal silicides, complete solid solutions form when the two binary silicides are isomorphic, and a partial solid solution or ternary compound forms when the two binary compounds are non-isomorphic [10]. $TiSi_2$ has an orthorhombic (C-54) structure with a packing sequence ABCD, and WS_2 has a tetragonal (C-11b) structure with a packing sequence ABAB. These two structures are not isomorphic, hence it is reasonable to expect that a ternary compound will form. Formation of ternary compounds has also been reported in both the Ti-Mo-Si system and the Ti-Re-Si system [10].

The Ti-W-Si system has been studied by Nowotny [11]. He reports a ternary disilicide of composition $Ti_{0.6}W_{0.4}Si_2$, observed in bulk samples prepared by high pressure sintering at 1300°C from a mixture of 58 Mol % $TiSi_2$ and 42 Mol % $TiSi_2$. However, Nowotny reports that with less than 58 Mol % $TiSi_2$ no compound forms and a two phase mixture of $TiSi_2$ and WSi_2 exists. In the present case, the equivalent of 30 Mol % of $TiSi_2$ is present and compound formation is observed. This discrepancy between Nowotny and the present work could possibly be due to the thin-film nature of the samples and the preparation used here.

The surface undulation after compound formation is probably due to the volume expansion the film experiences as a result of Si inclusion.

The film undergoes only a small density change from approximately 6.14×10^{22} atom/cm^3 calculated from the weighted sum of the elemental densities, to approximately 7.54×10^{22} atom/cm^3 calculated for the compound from the X-ray data.

A reduction of reaction rates by oxygen contamination has been observed by Kräutle [12] in the formation of VSi_2 by thin films of V on Si. It is remarkable that the rate of reaction is closely linear in spite of considerable oxygen contamination (see Figure 5). The observations that the rate remains linear at reduced oxygen contamination and that the substrate crystal orientation also influences the rate, is consistent with a reaction-limited mechanism. This hypothesis is further supported by the fact that Borders [4] reports linear rates for the WSi_2 formation. No published data exist for reaction rates of Ti films on Si substrates.

The extremely high activation energy of 4.5 eV may be a direct manifestation of the oxygen contamination. Sinha [13] reported an activation energy of 4.4 eV for WSi_2 growing at the expense of PtSi. The activation energy reported here may be the result of $Ti_{0.3}W_{0.7}Si_2$ growing at the expense of an oxide of titantium and/or tungsten. An argument against this hypothesis is the fact that no oxides of Ti or W were detected in the X-ray photographs. The X-ray analysis, though, is not very sensitive to small oxide concentrations over narrow regions such as the reaction interface. At present, the high apparent value of the activation energy is not understood.

The influence of deposition bias on the reaction rate may also be a contamination effect. The samples with -50V deposition bias had

both lower reaction rates and higher argon contamination levels than the sample deposited at zero bias. However, certain parameters of the films such as stress or crystal grain size which could influence the reaction rate were not well characterized. Differences in these parameters could also contribute to variations in reaction rates between samples prepared at different biases.

Since we were unable to perform annealing without introducing detectable amounts of contamination, the kinetics data presented here are to be considered preliminary. A final determination of the intrinsic kinetic behavior of Ti-W on Si will have to await the results of experiments with even lower contamination levels. It would also be worthwhile to extend this study to Ti-W films with various initial compositions, or to other disilicide-forming bimetal combinations. The results would be of value to the subject of ternary silicides in general, and to their possible application in silicon device technology in particular.

Interaction of Au on Ti-W

Many facets of the pitting and fracturing observed on Au/TiW/Si samples are not understood. The phenomenon is probably linked with the Au-Si eutectic at 371^{o}C [14] and with the surface migration of either Si or Au at low temperature. It seems clear that once either fractures or holes form, the Au migrates and accumulates there. Formation of the holes is probably at sites of pin-holes or other defects in the Ti-W layer. However, it is not clear whether the cracks form independently of the holes or whether the cracks are a later development initiated by hole formation. Some evidence exists which suggests that cracks form only as a result of the cooling after annealing.

A phenomenon similar to those observed above on Au/TiW/Si has been reported by Christov and Day [15] on the Au/Ti/Pt/Si system. They report that pin-hole formation is correlated with the fluoride ion concentration on the Si substrate prior to deposition and that failure is associated with high stress areas. They also mention that pin-hole formation is accelerated by F^{-} concentration on the Au/TiW/Si system. It is likely that film stress plays an important role in the failures observed in the Au/TiW/Wi system. The samples with -50V deposition bias are thought to be in compressional stress and those with 0 V bias in tensional stress. These measurements are rather qualitative, since they were made by observing the distortion of thin mica slabs on which a TiW layer was deposited at the two biases. On the other hand, the facture patterns correlate well with these stress measurements. On the Au/TiW/Si samples with -50V deposition bias, the pattern is linear in nature and on those with 0 V bias the pattern is polygonal. These patterns are characteristic of compressional and tensional stress respectively.

The important point is that the Au/TiW/Si metallization system is not stable at 350°C. The Ti-W film is not a barrier to the mixing as originally thought. Hence, use of this system for high temperature applications and its long term stability at any temperature is questionable.

REFERENCES

Part II

1. J. L. Vossen, J. Vacuum Sci. Technol. 11, 60 (1974).
2. J. A. Cunningham, IEEE Trans. on Reliability R19, 182 (1970).
3. L. D. Locker and C. D. Capio, J. Appl. Phys. 44, 4366 (1973); A. K. Sinha, M. H. Reed and T. E. Smith, J. Electrochem. Soc., Solid-State Science and Tech. 120, 1775 (1973).
4. J. A. Borders and J. N. Sweet, Proc. Intl. Conf. on Applications of Ion Beams to Metals, Albuquerque, New Mexico, 1973, Eds. S. T. Picraux, S. P. EerNisse and F. L. Vook (Plenum Press, New York, 1974), p. 179.
5. H. Kräutle, M-A. Nicolet and J. W. Mayer, p. 193 of Ref. 4. See also, Physica Status Solidi A 10, k33 (1973).
6. W. K. Chu, J. W. Mayer, M-A. Nicolet, T. M. Buck, G. Amsel and F. Eisen, Thin Solid Films 17, 1 (1973).
7. S. S. Lau, W. K. Chu, J. W. Mayer and K. N. Tu, Thin Solid Films 23, 205 (1974).
8. Andre Guinier, X-ray Crystallographic Technology, Hilgar and Watts Ltd., London, 1952.
9. C. C. Chang, Characterization of Solid Surfaces, Eds. Kane and Larrabee, (Plenum Press, New York, 1974), Chapter 20, p. 509.
10. H. J. Goldschmidt, Interstitial Alloys (Plenum Press, New York, 1967), Chapter 7, p. 323.
11. H. Nowotny, R. Kieffer and H. Schachner, M. L. Chem. 83, 1243 (1952).
12. H. Kräutle, M-A. Nicolet and J. W. Mayer, J. Appl. Phys. 45, 3304 (1974).
13. A. K. Sinha and T. E. Smith, J. Appl. Phys. 44, 3465 (1973).
14. W. Gerlach & B. Goel, Solid State Electronics 10 589-592 (1967).

15. A. Christov and H. M. Day, Electrochemical Society Extended Abstracts, Vol. 75-1, Spring 1975, Abstract #192, p. 455.

16. ASTM X-ray powder data file, American Society for Testing Materials, Philadelphia, Pa.

17. F. J. Biondi ed., Transistor Technology Vol. III (Van Nostrand, Inc., New York, 1958), p. 116.

APPENDIX I

Thin Solid Films, *19* (1973) 259–265

ENERGY STRAGGLING OF ^{4}He BELOW 2 MeV IN Pt*

J. M. HARRIS, W. K. CHU AND M-A. NICOLET
California Institute of Technology, Pasadena, Calif. 91109 (U.S.A.)
(Received August 10, 1973)

Energy straggling of ^{4}He has been measured in Pt films ranging from 200 to 4500 Å. The measurement was made by back-scattering spectrometry at energies below 2.0 MeV. The results lie between the predictions of Bohr's and Lindhard and Scharff's theories. Straggling is roughly proportional to the square root of the thickness, but also depends slightly on energy.

I. INTRODUCTION

In recent years, back-scattering spectrometry has been remarkably successful as a new microanalytical tool to sense mass, resolve depth and perceive monocrystalline structure in a solid simultaneously[1]. Energy straggling of the incident beam as it penetrates into the target limites the ultimate resolution of both mass and depth. To estimate these limits, the magnitude of energy straggling has to be known. The value depends on the beam particle, the beam energy and the target. He and H are the projectiles most commonly used for back-scattering analysis in the range of 1–2 MeV. For protons and solid targets some experimental results are available[2], but for He, data are scarce[3, 4]. We have undertaken to measure the energy straggling of He below 2 MeV for some representative elements. This paper reports on a series of measurements on Pt.

II. EXPERIMENTAL PROCEDURE AND ANALYSIS

Pt films were prepared by sputtering Pt onto substrates of thermally grown SiO_2 on Si wafers. The average mass per unit area was determined by differential weighing of the sample before and after deposition. Bulk density (21.4 g/cm^3) of Pt was used to arrive at the thickness of the films. In this manner, thicknesses of the films were determined to ± 40 Å. Thickness uniformity was checked by comparing back-scattering spectra of different parts of the samples. No significant variations were observed.

---

* Paper presented at the International Conference on Ion Beam Surface Layer Analysis, Yorktown Heights, New York, U.S.A., June 18–20, 1973.
Work supported in part by the Office of Naval Research.

^{4}He back-scattering spectra were taken in the range 1.0–2.0 MeV. A Si surface barrier detector with a resolution of less than 18 keV and a magnetic analyzer with a resolution of less than 5 keV were used. The data using the solid state detector was taken at an angle θ (see Fig. 1) of 168°. The magnetic analyzer used an angle of 150°.

The resolution of the detecting system and the energy straggling are obtained by analysis of the front and rear edges of a spectrum. The derivative of the front edge yields a gaussian-like function whose full width at half maximum (FWHM) is characteristic of the resolution of the system (see Fig. 1). The derivative of the rear edge yields a gaussian-like function whose FWHM is characteristic of the resolution of the system plus the energy straggling of that part of the beam which has traversed forth and back through the entire Pt film. For the analysis, it was assumed that these functions are true gaussians. The energy straggling ΔE

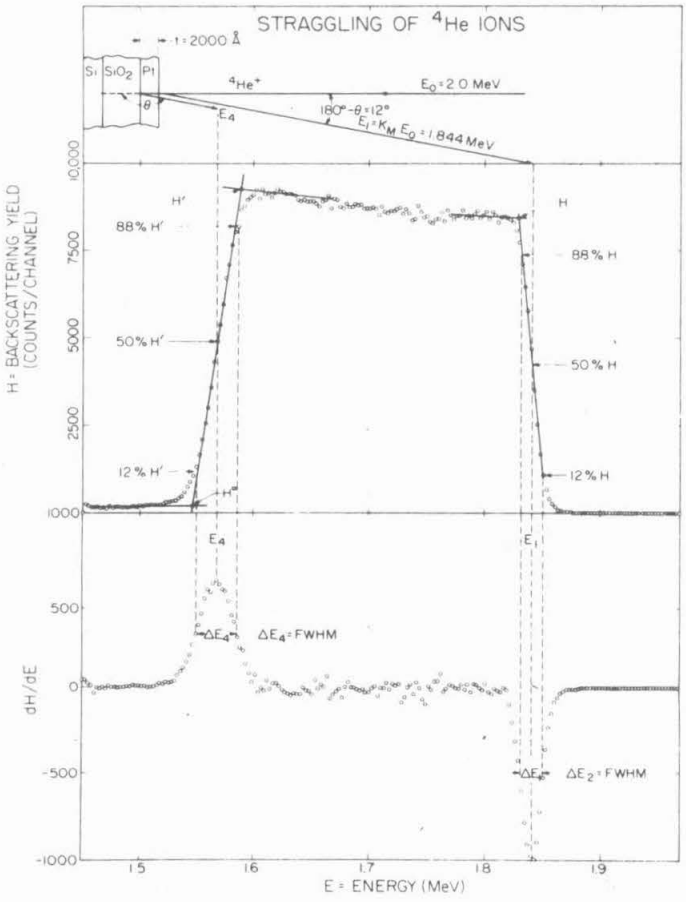

Fig. 1. Top: typical back-scattering spectrum of a 2000 Å Pt film taken with $^4He^+$ ions using a solid state detector. The signal of the SiO_2 substrate is not shown. Bottom: derivative of the above spectrum obtained by numerical methods. For a gaussian, the 50% points match the 12% and 88% points of the corresponding error function.

is then obtained by taking the difference in quadrature of the front edge FWHM, ΔE_1, and the rear edge FWHM, ΔE_4, *i.e.*

$$\Delta E^2 = \Delta E_4^2 - \Delta E_1^2 \tag{1}$$

Once it is assumed that the derivatives of the front and rear edges are gaussians, it becomes unnecessary to differentiate each spectrum. The FWHM can then be obtained directly from the edges as the difference in energy between the 12% and 88% points of the step height, as shown in Fig. 1 [5]. In the spectra of the thickest Pt films, the step height of the rear edge is ill defined because of significant background in the yield and a finite slope in the plateau of the Pt spectrum. Generally, therefore, the height of the step is measured from the average value H° of the background to the intersection point H'. This point is defined by the intersection of two lines, as shown in Fig. 1 (top). One of these lines is tangent to the inflection point of the edge; the other forms an extension of the plateau. A similar procedure is applied to define the step height H of the front edge.

In some cases, typically when the thickest films are measured at low energies, the differentiated rear edge of the spectrum differs from a gaussian. The resulting uncertainty contributes a main error in the final results. To estimate its magnitude, the energy at the 12% point of the step height, as defined above, was measured on both the inflection point tangent and on the actual curve of the edge. The difference of these two energies was taken and compared with the same quantity at the 88% point. When these two quantities differed by more than 5% of the FWHM, the straggling was recorded with a triangle in Figs. 2 and 3 to indicate a possible systematic error in that value. The main statistical error resides in the fact that energy differences cannot be read to much better than ± 1 channel, corresponding to ± 1.5 keV. In thick targets at low energies, the error in the step height due to uncertainties in the level of the background and the plateau also contributes to the statistical error; the effect is minor and never exceeds 50% of a channel. The error bars given in Figs. 2 and 3 have been obtained by adding these errors in quadrature, including the error propagation from eqn. (1).

III. RESULTS

In Fig. 2, the values of ΔE measured at incident beam energies of 1.0, 1.5 and 2.0 MeV are plotted against the square root of the film thickness t. The results obtained with the magnetic analyzer (open marks) and with the solid state detector (full marks) agree within expectation. The straight lines drawn through the experimental points show that the $\sqrt{t}$ dependence is followed fairly well.

The same experimental data are replotted in Fig. 3 to show the energy dependence of ΔE. The ordinate gives ΔE normalized with respect to $\sqrt{NZ_2 t}$, where N is the volume density of atoms (6.6×10^{22}cm^{-3}) and Z_2 is the atomic number (78) of Pt. This removes the dependence of ΔE on the thickness and on the electron density of the target, according to Bohr's theory[6], and displays the intrinsic energy dependence of the straggling. The abscissa gives the average energy $\bar{E}$ defined in such a manner that, formally, the energy width $E_1 - E_4$ of the Pt spectrum (see Fig. 1) is given to a first approximation by the expression

$$E_1 - E_4 = (K_{Pt} + |\cos^{-1}\theta|)Nt\ \varepsilon(\bar{E})$$

According to Moorhead[7]

$$\overline{E} = \frac{|\cos\theta|E_1 + E_4}{1 + K_{Pt}|\cos\theta|} \tag{2}$$

where K_{Pt} is the elastic scattering factor and $\varepsilon(E)$ is the stopping cross section of Pt (see Appendix).

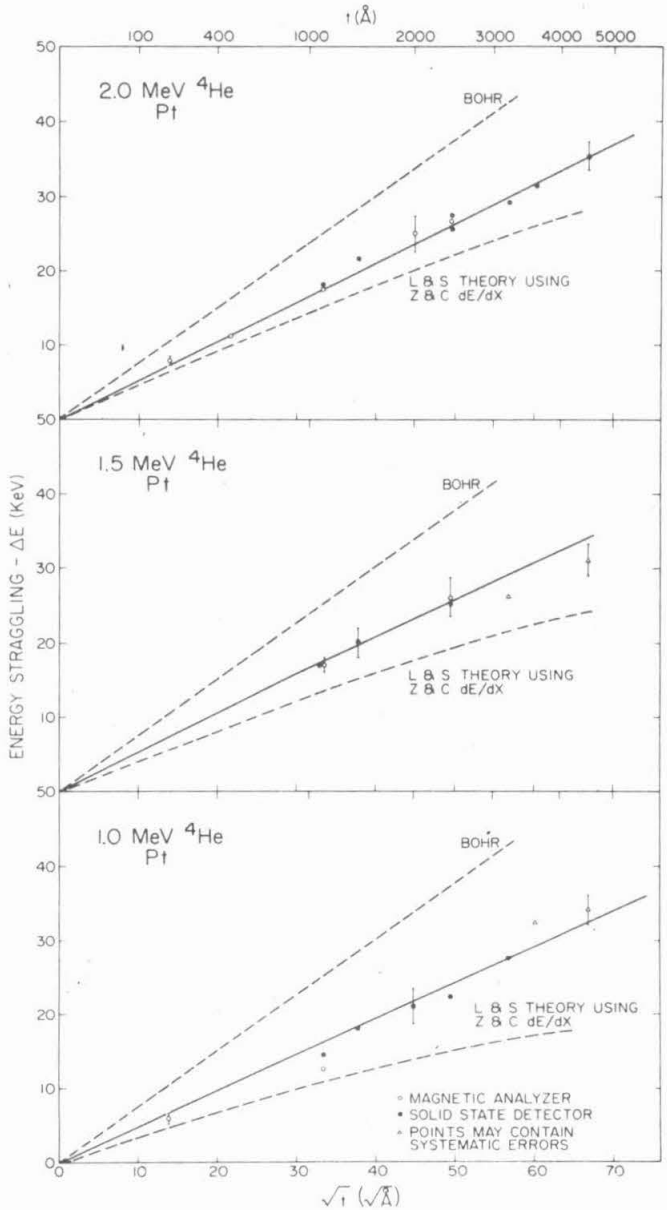

Fig. 2. Energy straggling of ^{4}He in Pt films at 1.0, 1.5 and 2.0 MeV as a function of the square root of their thickness. The broken lines show the predictions of Bohr's and Lindhard and Scharff's theories.

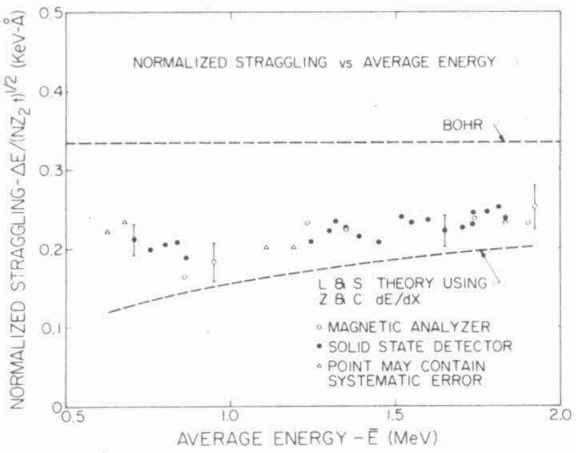

Fig. 3. Normalized straggling of ^{4}He in Pt films *vs.* average energy. The normalization removes the thickness dependence shown in Fig. 2.

Numerical information on the results of Figs. 2 and 3 is listed in Table I. Measurements performed with the magnetic analyzer are marked by an asterisk in the energy column. Data on $\Delta E/\Delta x$ are discussed in the Appendix.

TABLE I

t(Å)	E_0(MeV)	$E_1 = k_{Pt}E_0$	E_4(MeV)	$\bar{E}$	ΔE_2(keV)	ΔE_4(keV)	ΔE(keV)
4554	2.0	1.844	1.232	1.596	16.8	39.2	35.4
3747	2.0	1.844	1.333	1.650	16.8	35.0	30.5
3333	2.0	1.844	1.396	1.708	16.8	33.6	29.2
2532	2.0	1.844	1.494	1.734	16.8	30.8	25.9
2532	2.0	1.844	1.504	1.739	15.0	32.2	27.5
2532	2.0*	1.878	1.504	1.737	4.0	27.0	26.8
2005	2.0	1.844	1.579	1.779	15.0	27.4	25.1
1482	2.0	1.844	1.650	1.816	15.0	26.6	21.7
1482	2.0*	1.873	1.662	1.822	4.0	21.0	20.6
1170	2.0	1.844	1.689	1.837	15.0	23.8	18.2
1170	2.0*	1.870	1.709	1.847	4.0	18.0	17.6
483	2.0*	1.873	1.807	1.904	4.5	12.0	11.3
202	2.0*	1.876	1.847	1.926	6.0	10.0	8.0
2532	1.5*	1.406	1.014	1.237	4.0	18.0	26.1
1170	1.5*	1.407	1.222	1.354	6.0	18.0	17.0
4554	1.0	0.922	0.288	0.626	15.84	37.4	34.0
3747	1.0	0.922	0.380	0.674	15.84	36.0	32.4
3333	1.0	0.922	0.437	0.704	15.84	32.0	27.5
2532	1.0	0.922	0.534	0.755	15.84	27.3	22.3
2005	1.0	0.922	0.617	0.799	15.2	25.9	21.0
1482	1.0	0.922	0.695	0.839	14.4	23.0	18.0
1170	1.0	0.922	0.739	0.863	14.4	20.1	14.4
1170	1.0*	0.935	0.740	0.860	4.0	13.5	12.5
202	1.0*	0.933	0.902	0.949	4.0	6.2	5.8

Measurements were taken with a solid state detector at a back-scattering angle of 168°, except for those marked with an asterisk which were taken with a magnetic analyzer at a back-scattering angle of 150°.

IV. DISCUSSION AND CONCLUSION

The results given in Fig. 2 indicate that the simple $\sqrt{t}$ dependence of Bohr's theory fits the data quite well, but that numerically the theory over-estimates straggling by as much as 50%. On the other hand, Lindhard and Scharff's theory[8] predicts a value which is too low but fits the data a little closer. It must be pointed out, however, that this theory requires the knowledge of dE/dx for Pt so that these theoretical values are subject to the uncertainties in dE/dx[4]. To calculate the theoretical dependences according to Lindhard and Scharff which are plotted in Figs. 2 and 3, we have used the stopping power data of Ziegler and Chu[9] given in the Appendix.

The intrinsic energy dependence shown in Fig. 3 is weak. Because of the experimental errors, it is not possible to ascertain whether the data favor one or the other of the two theories. In this respect, our results are similar to those given by Nielsen[10] for protons and neutrons in certain metals.

We hope to reduce the errors of these results by improving the method of analysis and increasing the resolution of the detector system. We also intend to investigate elements other than Pt to test the dependence of energy straggling on the mass of the target element.

REFERENCES

1 W. K. Chu, J. W. Mayer, M-A. Nicolet, T. M. Buck, G. Amsel and F. Eisen, *Thin Solid Films*, *17* (1973) 1.
2 C. B. Madsen and P. Venkatesworlu, *Phys. Rev.*, *74* (1948) 1782;
C. B. Madsen, *Dan. Mat. Fys. Medd.*, *27* (1953) No. 13;
A. L. Morsell, *Phys. Rev.*, *135* (1964) A1436;
L. P. Nielsen, *Dan. Mat. Fys. Medd.*, *33* (1961) No. 6.
3 F. Demichelis, *Nuovo Cimento*, *13* (1959) 2134;
J. R. Comfort, J. F. Decker, E. T. Lynk, M. O. Scully and A. R. Quinton, *Phys. Rev.*, *150* (1966) 249;
D. A. Sykes and S. J. Harris, *Nucl. Instr. Methods*, *94* (1971) 39.
4 E. Bouderup and P. Hvelplund, Phys. Rev., *A4* (1971) 562.
5 P. R. Bevington, *Data Reduction and Error Analysis for the Physical Sciences*, McGraw-Hill, New York, 1969, pp. 305–309.
6 N. Bohr, *Dan. Mat. Fys. Medd.*, *18* (1948) No. 8.
7 R. D. Moorhead, *J. Appl. Phys.*, *36* (1965) 391.
8 J. Lindhard and M. Scharff, *Dan. Mat. Fys. Medd.*, *27* (1953) No. 15.
9 J. F. Ziegler and W. K. Chu, *IBM Res. Rept. RC 4288 (# 19193)*.
10 L. P. Nielsen, *Dan. Mat. Fys. Medd.*, *33* (1961) No. 6.

APPENDIX

To make calculations according to Lindhard and Scharff's theory it is necessary to know dE/dx as a function of energy. We have used the values of Ziegler and Chu[9] plotted in Fig. A1.

The direct method to obtain dE/dx data is to measure the energy loss ΔE of a given beam upon transmission through a self-supported thin film of thickness Δx.

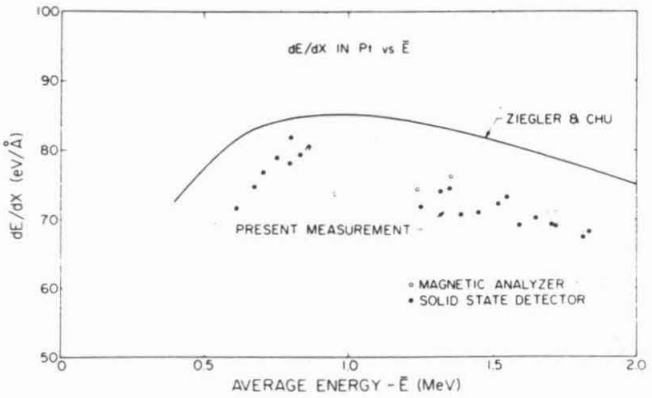

Fig. A1. The stopping power of ^{4}He in Pt as a function of energy, taken from Ziegler and Chu[9] (solid line), and used in our calculations. Also shown are preliminary experimental data obtained in this study.

The main difficulty is to prepare thin self-supported films. Back-scattering measurements on deposited thin films circumvent this target preparation problem. In this method, the energy loss contributed by both the incoming and the outgoing path of the particle trajectory is measured, so that a proper average energy has to be determined analytically[7]. The method works well as long as the incident energy E_0 and the detected energy E_4 do not straddle the maximum in the dE/dx curve. For these cases, values for dE/dx have been determined. They can be determined from Table I and are plotted in Fig. A1 [7]. The results are preliminary and error bars are not given. We hope to resolve the possible differences between the present measurement and those of Ziegler and Chu, thereby improving the reliability of the Lindhard and Scharff calculations.

APPENDIX II

PHYSICAL REVIEW B VOLUME 11, NUMBER 3 1 FEBRUARY 1975

Energy straggling of ^{4}He ions below 2.0 MeV in Al, Ni, and Au†

J. M. Harris and M-A. Nicolet
California Institute of Technology, Pasadena, California 91125
(Received 15 July 1974; revised manuscript received 14 October 1974)

Energy straggling of ^{4}He ions has been measured in thin films of Ni, Al, and Au. The observed straggling is roughly proportional to the square root of thickness and appears to have a slight energy dependence for all these materials. The results are compared with predictions of the theories of Bohr, Lindhard and Scharff, and of Chu and Mayer. Both the Ni and Au results are below the predictions of Bohr and are above the predictions of Chu and Mayer, and of Lindhard and Scharff. The Al measurements are above predictions of all these theories.

INTRODUCTION

In recent years, backscattering spectrometry has been remarkably successful as a microanalytical tool for sensing mass, resolving depth, and perceiving monocrystalline structure in solids.[1] Energy straggling of the incident beam as it penetrates the target limits the ultimate ability to resolve depth. To estimate these limits, the magnitude of energy straggling must be known. Energy straggling depends on target material, beam energy, and incident particle. He and H are the most common projectiles used for backscattering analysis in the energy range of 1–2 MeV. Experimental straggling data in solids are available for H,[2] but those for He are much more scarce.[3–6] Pt is the only element for which He straggling measurements below 2.0 MeV in thin films exist.[6] Yet this is just the region where backscattering spectrometry is typically used. Measurements of ^{4}He$^+$ energy straggling below 2.0 MeV made in thin Al, Ni, and Au films are reported here. These materials were selected as representative of light, medium, and heavy elements.

ANALYTICAL METHOD

Energy straggling results from the statistical nature of the energy-loss processes a particle experiences as it penetrates matter. If $f(E)$ denotes the energy distribution function at some depth of an initially monoenergetic beam, then energy straggling Ω is defined as the standard deviation of $f(E)$ with respect to the average. This distribution function, in general, is rather complicated and nonsymmetrical with respect to the mean.[7] However, $f(E)$ has been measured for thin targets and in this case found to be approximately a Gaussian function of energy.[6] For analysis of the present data, $f(E)$ is thus assumed to be Gaussian. The standard deviation Ω of a Gaussian is related to the full width at half-maximum (FWHM). The FWHM of $f(E)$, ΔE, is given by

$$\Delta E = (8 \ln 2)^{1/2} \Omega = 2.355 \Omega. \tag{1}$$

In experimental work ΔE is the quantity usually determined, whereas theories normally predict values for Ω.

Traditionally, energy straggling was measured by transmission of a monoenergetic beam of particles through a self-supporting thin foil or gas cell. In this configuration $f(E)$ is measured from the energy spectrum of the transmitted beam and Ω determined directly. This method relies on thin highly uniform self-supported films which are difficult to produce and handle. These problems are circumvented by measuring in a backscattering configuration, because the film can be deposited on a rigid substrate. The experiments reported here were performed in this configuration.

Measurements made in backscattering, however, are more complicated to interpret for two reasons: (i) The beam traverses the target more than once, and (ii) the particle energy distribution function is modified by the backscattering collision. To interpret straggling measurements made by backscattering one should first consider the straggling of a beam traversing two layers in succession. The resulting straggling is $(\Omega_A^2 + \Omega_B^2)^{1/2}$, where Ω_A and Ω_B are the straggling measured at the appropriate energies for layers A and B individually, and where the distributions are assumed to be Gaussian. In the backscattering configuration, Ω_B simply corresponds to the straggling generated in the outgoing path, Ω_{out}. The straggling generated in the incoming path, Ω_{in}, must be modified, since this path terminates with an elastic collision. It can be shown that the standard deviation of any particle energy distribution function is multiplied by K after an elastic collision, where K is the elastic-scattering factor. The straggling in backscattering configuration Ω_b is thus given by

$$\Omega_b^2 = K^2 \Omega_{in}^2 + \Omega_{out}^2. \tag{2}$$

In practice, the incident beam is not monoenergetic but has an energy profile with standard deviation Ω_{beam}. Furthermore, the fluctuations in the detection system can be characterized by a standard

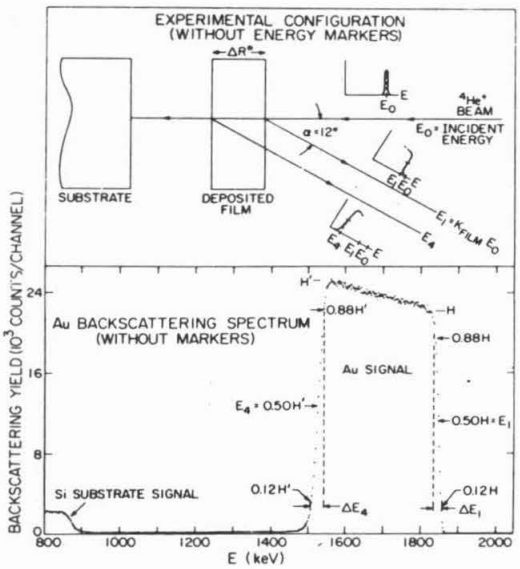

FIG. 1. Experimental configuration without energy markers and a typical backscattering spectrum of a Au target using $^4He^+$ ions and a solid-state detector.

deviation Ω_{det}. Both these standard deviations result from distributions which are closely Gaussian, so that the measured straggling value in backscattering configuration, Ω_4 is given by

$$\begin{aligned}\Omega_4^2 &= K^2(\Omega_{in}^2 + \Omega_{beam}^2) + \Omega_{out}^2 + \Omega_{det}^2 \\ &= K^2\Omega_{in}^2 + \Omega_{out}^2 + \Omega_1^2 \\ &= \Omega_b^2 + \Omega_1^2 ,\end{aligned} \tag{3}$$

where Ω_1^2 is the system resolution, given by

$$\Omega_1^2 = K^2\Omega_{beam}^2 + \Omega_{det}^2 .$$

Equation (3) can be expressed equivalently as

$$\Omega_b = (1/2.355)(\Delta E_4^2 - \Delta E_1^2)^{1/2} , \tag{4}$$

where ΔE_4 and ΔE_1 are the FWHM associated with Ω_4 and Ω_1.

For films of heavy monoisotopic and inert elements such as Au, ΔE_1 and ΔE_4 can be obtained from the backscattering spectrum taken on a target consisting simply of the film and an appropriate substrate. ΔE_1 is obtained from the high-energy edge of the spectrum, since this signal originates from that fraction of the beam which scatters from the surface ($\Omega_{in} = 0 = \Omega_{out}$). Similarly, ΔE_4 can be obtained from the low-energy edge of the spectrum, since this signal is due to particles which traverse the film completely (see Fig. 1). These edges display the integrals of the energy distrubution functions associated with ΔE_1 and ΔE_4, respectively. Since these functions are assumed to be Gaussians, ΔE_1 and ΔE_4 are the energy differences between the 12 and 88% points of the front and rear edges. (See Fig. 1 and Ref. 6 for further details.)

In films of low atomic weight the backscattered particles lose a significant fraction of their energy in the elastic collision. The incoming and outgoing particles thus lie in separate energy ranges, which complicates the interpretation of the measurement. This difficulty can be removed by using targets with energy markers. These markers are very thin layers of heavy metal such as Pt or Au which are vacuum deposited on both sides of the film under investigation. To be usable as a marker, a layer of heavy element must be so thin that the energy loss of the beam traversing it is small compared to ΔE_1. When this is so, the system resolution function and the energy profile of the backscattered beam, as sampled by the heavy element, will be displayed by the backscattering signals of the top and bottom markers, respectively. ΔE_1 and ΔE_4 can then be measured from these marker signals directly (see Fig. 2). Whether a marker is thin enough can be easily tested. As discussed above, ΔE_1 can be obtained from the leading edge of a backscattering signal of a heavy element such as Au. Consequently, a marker is sufficiently thin if it indicates a system resolution Ω_1 (or ΔE_1) which is indistinguishable from that measured on the high-energy edge of a clean Au target. All our heavy markers meet this criterion and have typically an areal density of about 6 $\mu g/cm^2$.

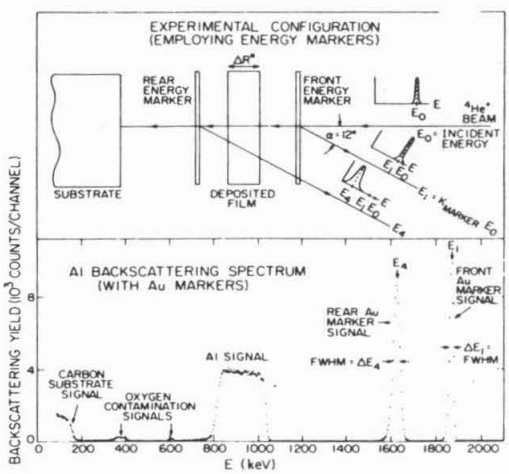

FIG. 2. Experimental configuration using energy markers and a typical backscattering spectrum of an Al dummy target using $^4He^+$ ions and a solid-state detector. Au energy markers and the target contamination level can be seen in the spectrum.

The beam loses energy both while traversing the film and during the backscattering collision. Therefore the straggling obtained is from a beam which has undergone energy loss. But since heavy markers were used for light elements, the incoming and outgoing particles lie in contiguous energy ranges and the measured straggling can be regarded as that observed for an average energy over the total path. The average energy chosen here, $\bar{E}$, is the same one used in calculating the stopping cross section $\epsilon_a(\bar{E})$ from a backscattering spectrum and is given by[8]

$$\bar{E} = (E_1 \cos\alpha + E_4)/(1 + K\cos\alpha) , \qquad (5)$$

where E_0 is the mean energy of the incident beam, E_1 is the mean energy of the front marker signal, $E_1 = K E_0$, E_4 is the mean energy of the rear marker signal, K is the elastic-scattering factor for the marker material ($K_{Pt} = 0.922$, $K_{Au} = 0.923$), and α is the scattering angle (less than 90°) measured with respect to the beam (= 12°) (see Fig. 1).

This average energy reduces to the arithmetic average of E_0 and E_4 if $\alpha = 0$ and $K = 1$ (corresponding to an infinitely heavy marker). When energy-straggling measurements are made by transmission, the average energy used is the arithmetic average of the mean incident-beam energy E_0 and the mean transmitted-beam energy (analogous to E_4 in a backscattering configuration). $\bar{E}$ is thus analogous to the average energy used in transmission experiments. The energy dependence of straggling is weak, however, and the definition of $\bar{E}$ has little influence on the results.

EXPERIMENTAL PROCEDURE

A. Sample preparation

Depositions were all made by electron-gun evaporation onto clean polished substrates in an oil-free vacuum system at pressures lower than 1×10^{-6} Torr. Dummy samples on vacuum-baked polished carbon substrates were prepared simultaneously with the targets. The dummies were used to check for light contaminants, such as oxygen, in the films. Film thicknesses were measured with a multiple-beam interferometer.

Ni samples were prepared by first depositing a Pt marker on a Si substrate and then annealing at 280 °C for about $\frac{1}{2}$ h in a dry N_2 atmosphere. The Pt reacts with the substrate and forms PtSi.[9] This prevents the Pt from mixing with Ni during the subsequent Ni evaporation. The Ni film and top marker were deposited sequentially without breaking vacuum.

Al samples were prepared by sequentially depositing onto Si or SiO_2 substrates a Au marker, an Al film, and a top Au marker without breaking vacuum. Precautions against mixing were not necessary, probably because small amounts of Al_2O_3 form in the initial stages of the Al evaporation, creating a diffusion barrier between Au and Al.

Au targets were prepared by evaporation of Au onto Si substrates.

The straggling measurements presented here were performed in a backscattering configuration with the 3.0 MeV Van de Graaf accelerator in the Kellogg Radiation Laboratory. The energy analysis of the backscattered particles was made using a Si surface barrier detector followed by a commercial preamplifier, linear amplifier, and multichannel analyzer.

B. Sample and apparatus evaluation

Since the quality of the samples is critical to straggling measurements, the samples were examined for defects which might lead to erroneous results. Among the properties investigated were contamination level, lateral uniformity, surface roughness, and temperature stability.

Contamination was checked by backscattering spectrometry on the dummy samples, and oxygen was found to be the chief contaminant. Other impurities were either lighter than C or present in concentrations too small to be detected (see Fig. 2). By far the highest oxygen contamination was found in the Al samples (typically 2 at.%). Contamination by oxygen at these concentrations, however, should not influence the straggling in any significant way.

To ascertain lateral uniformity, backscattering spectra taken from different parts of the sample were compared. The samples were found to be uniform within 2%.

The surface roughness was investigated with a scanning electron microscope. The surface of the sample appeared featureless. Any surface irregularities present were below the resoltuion of the microscope used (~400 Å). Surface roughness was not investigated further because previous investigations using a tally step (resolution ~ 100 Å) on Cr samples prepared similarly revealed that samples made on polished Si substrates were smooth to the order of the instrument resolution. Further indication that surface irregularities are small is given by the square root of thickness dependence of the straggling measurements, as it seems rather unlikely that surface roughness would significantly influence the measurements and leave the square root of thickness dependence unchanged.

The temperature stability of the films was investigated by annealing a completed target in a dry N_2 atmosphere for $\frac{1}{2}$ h at 200 °C. No change in the backscattering signal was noted.

Examination of the Al targets after irradiation

with an optical microscope revealed small blisters in the film. Their height was measured by Newton rings, and from estimates of their typical shape, size, and number it was determined that no significant errors were introduced in the straggling measurement by them. Al targets were also prepared on SiO_2 substrates and no blistering occurred on these samples. Data from both sets of samples are given in the results.

Experiments were made to investigate the possible influence on the measurements of carbon deposition on the target during irradiation, and of irradiation itself. To this end, spectra taken at various beam currents (5–50 nA) for various lengths of time (0.25–2 h) and with various beam sizes (1–10 mm^2) were compared with one another. No significant differences were observed in the straggling evaluated from these spectra.

The stability and linearity of the backscattering apparatus were checked by taking a backscattering spectrum of various elements ranging from C to Pt with the beam at a given energy E_0. The front-edge energy E_1 of each element can be expressed

$$E_1 = K_{\text{element}} E_0 \tag{6}$$

(see Fig. 1). If the beam energy is stable and the energy detection system is linear and stable, a plot of the calculated energy E_1 versus the channel number corresponding to the front-edge 50%-height point should yield a straight line. The apparatus was found to be sufficiently linear and stable (deviations $< 0.5\%$ for irradiation times in excess of 18 h) to perform the straggling measurements. These last tests were performed *in situ* during straggling measurements for each set of samples.

THEORY

Several theories are available to describe energy straggling. The simplest is Bohr's theory,[10] according to which

$$\Omega_B^2 = (q^4/4\pi\epsilon_0^2) Z_1^2 N Z_2 \Delta R, \tag{7}$$

where q is the electronic charge, 1.60×10^{-19} C, $\epsilon_0 = 8.85\times10^{-12}$ F/m, Z_1 is the atomic number of the incident ion, Z_2 is the atomic number of the target material, ΔR is the ion path length, and N is the atom density of the target. Bohr's theory was derived assuming that (i) the target atoms are randomly distributed, (ii) the energy loss during a single interaction is very much less than the total energy loss over the entire path, and (iii) the projectile velocity is much greater than the orbital electron velocity of the target atoms. At low and medium energies this last assumption breaks down.

Lindhard and Scharff[11] have extended Bohr's theory by applying a correction factor for low- and medium-energy projectiles. Applying this correction, the energy straggling becomes

$$\begin{aligned} \Omega_{LS}^2 &= \Omega_B^2 \quad \text{for} \quad \omega = v^2/v_0^2 Z_2 > 3, \\ \Omega_{LS}^2 &= \Omega_B^2(\tfrac{1}{2}L) \quad \text{for} \quad \omega \leq 3, \end{aligned} \tag{8}$$

where $v_0 = q^2/4\pi\epsilon_0 h$ is the electron velocity in the first Bohr orbital of a hydrogen atom, v is the velocity of the projectile, and L is the stopping number of the target material.

The value of L can be determined experimentally from the stopping cross section,

$$\epsilon_\alpha = (Z_1^2 q^4/4\pi\epsilon_0^2 m v^2) Z_2 L, \tag{9}$$

where ϵ_α is the stopping cross section of the target material α and m is the mass of the electron, 9.108×10^{-31} kg, or, based on the Thomas-Fermi model of the atom, L can be approximated by

$$L = 1.36\ \omega^{1/2} - 0.016\ \omega^{3/2}. \tag{10}$$

The last formula [Eq. (10)] was used in the calculation of Ω_{LS} (Fig. 6) so that the theory would be independent of ϵ_α. This is convenient since ϵ_α values quoted in the literature are uncertain; see, for instance, Ref. 15 with respect to Au.

A refinement of the Lindhard-Scharff calculation was made by Bonderup and Hvelplund.[12] This refinement assumes a spherically symmetric radial charge distribution, namely, the first-order Lenz-Jensen model.[13] Chu and Mayer[14] have made further refinements by introducing the Hartree-Fock-Slater model for the radial charge distribution into the formalism generated by Bonderup and Hvelplund. This calculation of Chu and Mayer shows the Z_2 oscillation characteristic of using the Hartree-Fock-Slater wave functions and has an energy dependence similar to that of the Lindhard-Scharff theory.

Applying Bohr's theory to the backscattering configuration yields [Eqs. (2) and (7)]

$$\begin{aligned} \Omega_{bB}^2 = K^2\Omega_{B,\text{in}}^2 + \Omega_{B,\text{out}}^2 &= \frac{q^4}{4\pi\epsilon_0^2} Z_1^2 N Z_2 \\ &\times\left(K^2 + \frac{1}{\cos\alpha}\right)\Delta R^*, \end{aligned} \tag{11}$$

where ΔR^* is the thickness of the film.

In the remaining theories discussed, straggling is energy dependent. To calculate Ω_b with them, one can compute Ω_{in} and Ω_{out} independently at the average energy of each path and apply Eq. (2). Alternatively, one may calculate the straggling for the total path length, at the average energy $\bar{E}$ of Eq. (5). The result should be insensitive to the mode of calculation used because (i) the calculations are for thin targets, (ii) the calculations are for heavy targets or targets with heavy markers both

TABLE I. Measurements taken at a backscattering angle of 12° with a solid-state detector. Samples were made on Si substrates, with the exception of those marked +, which were made with SiO_2 substrates.

$\rho\Delta R^*$ (μg/cm^2)	E_0 (keV)	E_1 (keV)	E_4 (keV)	$\bar{E}$	ϵ_α	ΔE_1 (keV)	ΔE_4 (keV)	Ω (keV)
Al	$\rho = 2.7$ g/cm^3		$N = 6.0\times10^{22}$ atoms/cm^3				with Au markers	
32.96	2000	1846	1778	1883	47.93	18.84	22.77	5.44
59.08+	2000	1846	1726	1856	46.90	20.34	27.12	7.63
96.77	2000	1846	1649	1815	47.02	18.84	29.19	9.49
126.39+	2000	1846	1577	1778	48.89	19.44	33.22	11.46
32.96	1500	1385	1313	1411	50.67	18.48	23.35	6.04
59.08+	1500	1385	1253	1370	51.67	19.10	26.59	7.87
96.77	1500	1385	1165	1324	52.61	18.48	29.06	9.53
126.39+	1500	1385	1084	1282	55.16	19.90	33.29	11.36
32.96	1000	923	841	916	56.84	17.87	22.74	5.98
59.08+	1000	923	773	881	58.78	16.87	25.74	7.03
96.77	1000	923	677	830	66.95	18.44	28.60	9.30
Ni	$\rho = 8.9$ g/cm^3		$N = 9.13\times10^{22}$ atoms/cm^3				with Pt markers	
113.4	2000	1844	1688	1835	68.88	21.60	28.32	7.80
331.9	2000	1844	1381	1674	58.31	19.92	37.92	13.73
458.4	2000	1844	1213	1585	57.54	20.16	42.96	16.15
113.4	1500	1383	1220	1352	72.28	18.72	26.00	7.65
215.9	1500	1383	1062	1269	74.47	18.32	29.94	10.07
331.9	1500	1383	900	1184	72.90	18.12	32.51	11.48
458.4	1500	1383	743	1002	...	18.52	38.81	14.50
215.9	1000	922	590	784	76.67	16.44	27.74	9.50
458.4	1000	922	443	707	71.90	16.87	31.17	11.15
Au	$\rho = 19.3$ g/cm^3		$N = 5.9\times10^{22}$ atoms/cm^3				no markers	
165.98	2000	1846	1737	1870	110.80	18.78	25.31	7.22
330.41	2000	1846	1621	1800	117.37	19.21	30.06	9.58
464.55	2000	1846	1526	1750	116.02	21.02	33.67	11.20
1180.00	2000	1846	923	1430	121.59	22.82	50.85	19.33
165.98	1500	1385	1266	1380	120.76	18.12	22.66	5.78
330.41	1500	1385	1143	1300	126.55	26.59	33.88	8.93
464.55	1500	1385	1037	1260	126.02	18.71	30.93	10.48
1180.00	1500	1385	506	978	125.28	22.51	49.77	18.89
165.98	1000	923	801	895	117.33	16.87	21.59	5.73
330.41	1000	923	676	830	128.81	16.87	26.03	8.42
464.55	1000	923	577	778	125.28	16.87	28.46	9.74

of which have incoming and outgoing paths in adjacent energy ranges, and (iii) the theoretical energy dependences are intrinsically weak. Nevertheless, both methods were used and the results were compared. The differences were found to be insignificant (< 0.05%), as expected.

RESULTS

Results of measurements are given in Table I and plotted in Figs. 3–5. Plotted along with the data are straggling values calculated using Bohr's theory. Figures 3–5 and Table I are presented using areal density $\rho\Delta R^*$ where ρ is the bulk density, rather than the thickness ΔR^*. This was done to conform with presentations used in the bulk of the literature.

Energy straggling in all three elements is roughly proportional to square root of thickness, as predicted by Bohr. Measurements in Ni roughly agree with the Bohr theory, while in Al they are about 30% above and in Au about 40% below this theory.

The Au measurements are similar to previous measurements made in Pt.[6] This was expected since Pt and Au are neighboring elements in the periodic table. The straggling results in Al are similar to the results of Demichelis[4] and Sykes,[5] whose values are also higher than Bohr's theory. However, their data apply to much thicker films (~ mg/cm^2) and higher energies (~ 5 MeV), so that direct comparison is somewhat difficult. The situation is similar for Ni in that previous measurements[3] have been made at much higher energies and with thicker films.

In order to display the energy dependence of straggling it is convenient to plot $\Omega/(NZ_2\Delta R^*)^{1/2}$ since this reduces Bohr's theory to a universal curve. Figure 6 displays $\Omega/(NZ_2\Delta R^*)^{1/2}$ vs $\bar{E}$ for all three elements and the theories of Bohr,[10]

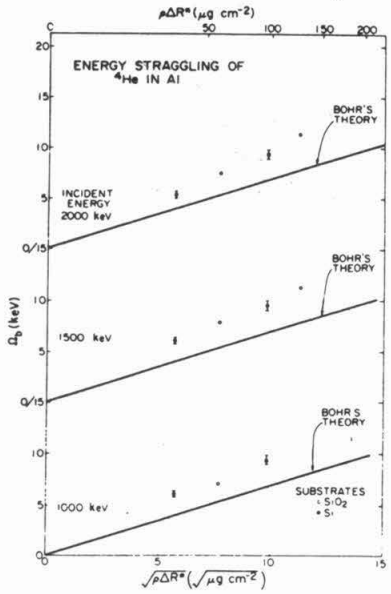

FIG. 3. Energy straggling of ^{4}He in Al films at incident energy of 1000, 1500, and 2000 keV as a function of the square root of areal density $\rho\Delta R^*$, where ΔR^* is the film thickness and ρ is the density. Solid line shows predictions of Bohr's theory.

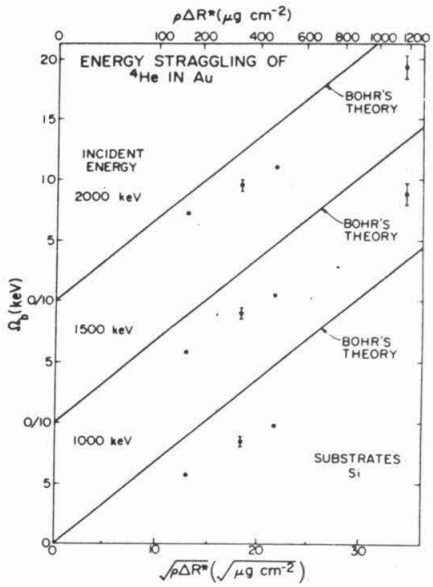

FIG. 5. Energy straggling of ^{4}He in Au films at incident energy of 1000, 1500, and 2000 keV as a function of the square root of areal density $\rho\Delta R^*$, where ΔR^* is the film thickness and ρ is the density. The solid line shows predictions of Bohr's theory.

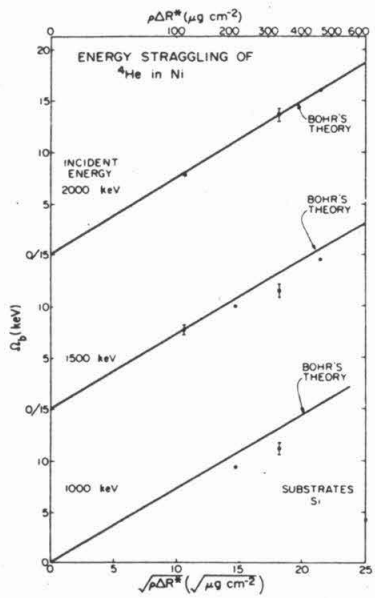

FIG. 4. Energy straggling of ^{4}He in Ni films at incident energy of 1000, 1500, and 2000 keV as a function of the square root of areal density $\rho\Delta R^*$, where ΔR^* is the film thickness and ρ is the density. Solid lines show predictions of Bohr's theory.

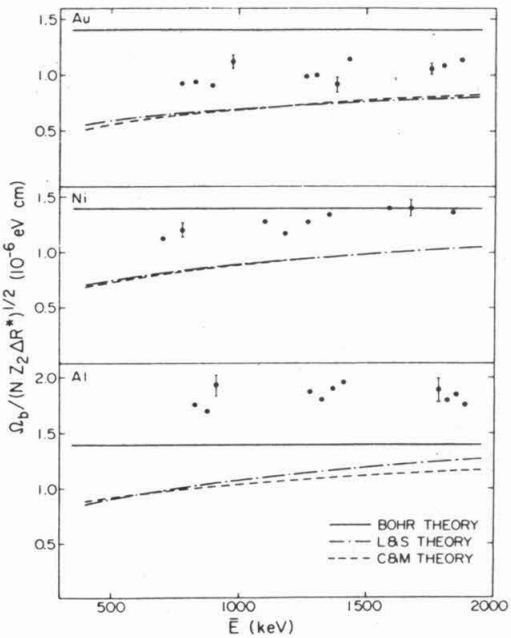

FIG. 6. Normalized straggling of ^{4}He in Al, Ni, and Au vs average energy, including the theories of Bohr (Ref. 10), Lindhard and Scharff (Ref. 11), and Chu and Mayer (Ref. 14).

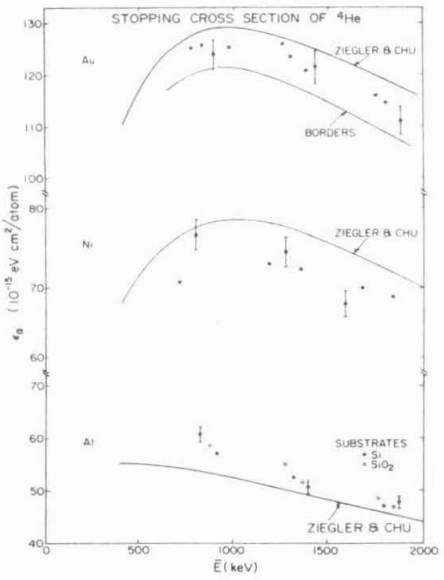

FIG. 7. Stopping cross section as a function of average energy for Al, Ni, and Au. Solid lines are values taken from Ziegler and Chu (Ref. 15) and Borders (Ref. 15).

Lindhard and Scharff,[11] and Chu and Mayer.[14] These last two theories qualitatively describe the observed energy dependence of straggling. However, the predictions of both theories are below the measurements for all three elements. Based on the data presented, it is not clear which theory gives the most accurate description of energy straggling.

The main statistical error in these measurements originates from the energy differences ΔE_1 and ΔE_4, which cannot be determined to better than ± 2.0 keV. This error, when added in quadrature with smaller statistical errors and propagated, yields an estimated uncertainty of about 10% in Ω. Representative error bars are given for Ω in Figs. 3–5. Error bars for the thickness are omitted in these figures since the resulting uncertainty in the abscissa (~2.5%) is typically the size of the symbol used.

To check for systematic errors in the measurements, ϵ_α was calculated from the backscattering spectra[8] and compared with current values in the literature.[15] Both the literature values and those from the backscattering spectra are shown in Fig. 7. The error bars given here arise from uncertainties in E_1, E_4, and the thickness of the films (~6% total). This check revealed no significant systematic errors since ϵ_α agrees with literature values within about 8% on the average.

CONCLUSION

Energy straggling of ^{4}He ions in Al, Ni, and Au, for the energy range of this experiment is roughly proportional to square root of thickness, as predicted by Bohr's theory. While Ni measurements are in fair agreement with this theory, Al measurements are about 30% above and Au measurements about 40% below predicted values. A weak dependence in straggling for these elements is qualitatively described by the theories of Lindhard and Scharff, and Chu and Mayer. These latter two theories underestimate the straggling in all three elements.

ACKNOWLEDGMENTS

We are grateful to J. S. Feng for supplying some samples and suggesting the use of markers and would like to thank W. K. Chu for providing his theoretical calculations. We also appreciate the assistance of D. S. Harris, M. E. Rienstra, and L. G. Scroggs in the preparation of the manuscript.

---

†Work supported by the Office of Naval Research (L. Cooper).

[1]W. K. Chu, J. W. Mayer, M-A. Nicolet, T. M. Buck, G. Amsel, and F. Eisen, Thin Solid Films 17, 1 (1973).

[2]C. B. Madsen and P. Venkatesworlu, Phys. Rev. 74, 1782 (1948); C. B. Madsen, K. Dan. Vidensk. Selsk. Mat.-Fys. Medd. 27, 13 (1953); L. P. Nielsen, *ibid.* 33, 6 (1961).

[3]J. R. Comfort, J. E. Decker, E. T. Lynk, M. O. Scully, and A. R. Quinton, Phys. Rev. 150, 249 (1966).

[4]F. Demichelis, Nuovo Cimento 13, 2134 (1959).

[5]D. A. Sykes and S. J. Harris, Nucl. Instrum. Methods 94, 39 (1971).

[6]J. M. Harris, W. K. Chu, and M-A. Nicolet, Thin Solid Films 19, 259 (1973).

[7]L. Landau, J. Phys. 8, 201 (1944); C. Tschalär, Nucl. Instrum. Methods 61, 141 (1968); J. J. Kolata, Phys. Rev. 176, 484 (1968).

[8]R. D. Moorhead, J. Appl. Phys. 36, 391 (1965); W. D. Warters, Ph.D. dissertation (Caltech, 1953) (unpublished).

[9]A. Hiraki, M-A. Nicolet, and J. W. Mayer, Appl. Phys. Lett. 18, 178 (1971).

[10]N. Bohr, K. Dan. Vidensk. Selsk. Mat.-Fys. Medd. 18, 8 (1948).

[11]J. Lindhard and M. Scharff, K. Dan. Vidensk. Selsk. Mat. Fys. Medd. 27, 15 (1953).

[12]E. Bonderup and P. Hvelplund, Phys. Rev. A 4, 562 (1971).

[13]H. Jensen, Z. Phys. 77, 702 (1932).

[14]W. K. Chu and J. W. Mayer (unpublished).

[15]J. F. Ziegler and W. K. Chu (unpublished); Thin Solid Films 19, 281 (1973); J. A. Borders, Radiat. Eff. 16, 253 (1972).